JHEP

Published for SISSA by Springer

Received: April 7, 2021
Revised: June 24, 2021
Accepted: July 8, 2021
Published: July 26, 2021

JHEP07(2021)195

Fitting the $Zb\bar{b}$ vertex in the two-Higgs-doublet model and in the three-Higgs-doublet model

Darius Jurčiukonis[a] **and Luís Lavoura**[b]

[a] *Vilnius University, Institute of Theoretical Physics and Astronomy, Saulėtekio ave. 3, Vilnius 10257, Lithuania*

[b] *Universidade de Lisboa, Instituto Superior Técnico, CFTP, Av. Rovisco Pais 1, 1049-001 Lisboa, Portugal*

E-mail: darius.jurciukonis@tfai.vu.lt, balio@cftp.tecnico.ulisboa.pt

Abstract: We investigate the new contributions to the parameters g_L and g_R of the $Zb\bar{b}$ vertex in a multi-Higgs-doublet model (MHDM). We emphasize that those contributions generally worsen the fit of those parameters to the experimental data. We propose a solution to this problem, wherein g_R has the opposite sign from the one predicted by the Standard Model; this solution, though, necessitates light scalars and large Yukawa couplings in the MHDM.

Keywords: Phenomenological Models

ArXiv ePrint: 2103.16635

Open Access, © The Authors.
Article funded by SCOAP[3].

https://doi.org/10.1007/JHEP07(2021)195

Contents

JHEP07(2021)195

1 Introduction

In this paper we focus on the $Zb\bar{b}$ coupling

$$\mathcal{L}_{Zbb} = \frac{g}{c_w} Z_\mu \bar{b}\gamma^\mu \left(g_L P_L + g_R P_R\right) b, \tag{1.1}$$

where c_w is the cosine of the weak mixing angle and P_L and P_R are the projection operators of chirality. At tree level,

$$g_L^{\text{tree}} = \frac{s_w^2}{3} - \frac{1}{2}, \quad g_R^{\text{tree}} = \frac{s_w^2}{3}, \tag{1.2}$$

where s_w is the sine of the weak mixing angle. With $s_w^2 = 0.22337$ [1], one obtains $g_L^{\text{tree}} = -0.42554$ and $g_R^{\text{tree}} = 0.07446$. The Standard Model (SM) prediction is [2]

$$g_L^{\text{SM}} = -0.420875, \quad g_R^{\text{SM}} = 0.077362. \tag{1.3}$$

In the presence of New Physics, we write

$$g_L = g_L^{\text{SM}} + \delta g_L, \quad g_R = g_R^{\text{SM}} + \delta g_R. \tag{1.4}$$

Experimentally, we get at g_L and g_R by measuring two quantities called A_b and R_b; their precise experimental definitions may be found in refs. [2–4] and in appendix A. One has

$$A_b = \frac{2r_b\sqrt{1-4\mu_b}}{1-4\mu_b+(1+2\mu_b)\,r_b^2}, \tag{1.5}$$

where $r_b = (g_L+g_R)/(g_L-g_R)$ and $\mu_b = \left[m_b\left(m_Z^2\right)\right]^2 \Big/ m_Z^2$. We use the numerical values $m_b\left(m_Z^2\right) = 3\,\text{GeV}$ and $m_Z = 91.1876\,\text{GeV}$ [1]. Equation (1.5) may be inverted to yield

$$\frac{g_L}{g_R} := \varrho = \frac{\sqrt{1-4\mu_b}\left[1 \pm \sqrt{1-(1+2\mu_b)\,A_b^2}\right] + (1+2\mu_b)\,A_b}{\sqrt{1-4\mu_b}\left[1 \pm \sqrt{1-(1+2\mu_b)\,A_b^2}\right] - (1+2\mu_b)\,A_b}. \tag{1.6}$$

Notice the existence of two solutions for ϱ. The other measured quantity is

$$R_b = \frac{s_b\,c^{\text{QCD}}\,c^{\text{QED}}}{s_b\,c^{\text{QCD}}\,c^{\text{QED}} + s_c + s_u + s_s + s_d}, \tag{1.7}$$

where $c^{\text{QCD}} = 0.9953$ and $c^{\text{QED}} = 0.99975$ are QCD and QED corrections, respectively,

$$s_b = (1-6\mu_b)\,(g_L-g_R)^2 + (g_L+g_R)^2 \tag{1.8a}$$

$$= g_R^2\left[(2-6\mu_b)\left(1+\varrho^2\right) + 12\mu_b\varrho\right], \tag{1.8b}$$

and $s_c + s_u + s_s + s_d = 1.3184$. The solution to equations (1.7) and (1.8b) is

$$g_R^2 = \frac{s_c+s_u+s_s+s_d}{c^{\text{QCD}}c^{\text{QED}}\left[(2-6\mu_b)\,(1+\varrho^2)+12\mu_b\varrho\right]}\,\frac{R_b}{1-R_b}. \tag{1.9}$$

Notice the two possible signs of g_R in equation (1.9).

An overall fit of many electroweak observables gives [4]

$$R_b^{\text{fit}} = 0.21629 \pm 0.00066, \tag{1.10a}$$

$$A_b^{\text{fit}} = 0.923 \pm 0.020. \tag{1.10b}$$

On the other hand, A_b has been directly measured at LEP1 and at SLAC in two different ways, see appendix A. The averaged result of those measurements is

$$A_b^{\text{average}} = 0.901 \pm 0.013. \tag{1.11}$$

While the A_b value of equation (1.10b) deviates from the Standard-Model A_b value 0.9347 by just 0.6σ, the A_b value of equation (1.11) displays a much larger disagreement of 2.6σ.

In this work we consider both the set of values (1.10), which we denote through the superscript "fit," and the set formed by the values (1.10a) and (1.11), which we denote through the superscript "average." Plugging the central values of those two sets into equations (1.6) and (1.9), we obtain solutions 1, 2, 3, and 4 for g_L and g_R in table 1. We also display in that table the corresponding values of $\delta g_L = g_L + 0.420875$ and $\delta g_R = g_R - 0.077362$. We

JHEP07(2021)195

solution	g_L	g_R	δg_L	δg_R
1^{fit}	−0.420206	0.084172	0.000669	0.006810
2^{fit}	−0.419934	−0.082806	0.000941	−0.160168
3^{fit}	0.420206	−0.084172	0.841081	−0.161534
4^{fit}	0.419934	0.082806	0.840809	0.005444
1^{average}	−0.417814	0.095496	0.003061	0.018134
2^{average}	−0.417504	−0.094139	0.003371	−0.171501
3^{average}	0.417814	−0.095496	0.838688	−0.172858
4^{average}	0.417504	0.094139	0.838379	0.016777

Table 1. The results of equations (1.6) and (1.9) for g_L and g_R and the corresponding values of δg_L and δg_R extracted from equations (1.3) and (1.4). The superscript "fit" corresponds to the input values (1.10), while the superscript "average" corresponds to the input values (1.10a) and (1.11).

see that solutions 3 and 4 have a much too large δg_L; we outright discard those solutions.[1] Solution 1 seems to be preferred over solution 2 because it has much smaller $|\delta g_R|$.[2] Still, in this work we shall also consider solution 2.

In this paper we seek to reproduce solutions 1 and 2 by invoking New Physics, specifically either the two-Higgs-doublet model (2HDM) or the three-Higgs-doublet model (3HDM). The 2HDM is one of the simplest possible extensions of the SM. One of the many motivations for the 2HDM is supersymmetry: the Minimal Supersymmetric Standard Model has two Higgs doublets. Also, the 2HDM may generate a Baryon Asymmetry of the Universe sufficiently large, due to the flexibility of its scalar mass spectrum. We recommend the review [7] on the 2HDM in general, and refs. [8, 9] on the aligned 2HDM. In recent years the 3HDM has received increased attention, see e.g. refs. [10–12]. The aligned 3HDM is discussed in refs. [9, 13].

The plan of this work is as follows. In section 2 we present the general formulas of δg_L and δg_R in the n-Higgs-doublet model. In section 3 we consider the particular case of an aligned 2HDM and we specify the constraints on the scalar masses that we have used in that case. We do the same job for an aligned 3HDM in section 4. We then present numerical results in section 5, followed by our conclusions in section 6. Appendix A deals on the definition of R_b and A_b and on the experimental data for them. Appendix B works out the derivation of the neutral-scalar contributions to δg_L and δg_R.

[1] Solutions 3 and 4 are good when one only measures R_b and A_b at the Z^0 peak; when one gets away from that peak, the diagram with an intermediate photon becomes significant and one easily finds that solutions 3 and 4 are not really experimentally valid [5]. So, there are both theoretical and experimental reasons for discarding them.

[2] A recent preprint [6] claims that there are already a couple LHC points that favour solution 1 over solution 2 and that in the future the two solutions could be decisively discriminated through the high-luminosity-LHC data. On the other hand, the older ref. [5] claims that the PETRA (35 GeV) data actually favour solution 2 over solution 1.

JHEP07(2021)195

2 The $Zb\bar{b}$ vertex in the aligned nHDM

2.1 Mixing formalism

In a general n-Higgs-doublet model (nHDM) and utilizing, without loss of generality, the 'charged Higgs basis' [14], the scalar doublets $\Phi_1, \ldots \Phi_n$ are written

$$\Phi_1 = \begin{pmatrix} S_1^+ \\ (v + H + iS_1^0)/\sqrt{2} \end{pmatrix}, \quad \Phi_k = \begin{pmatrix} S_k^+ \\ (R_k + iI_k)/\sqrt{2} \end{pmatrix} \quad (k = 2, \ldots, n), \tag{2.1}$$

where S_1^+ is a charged Goldstone boson, S_1^0 is the neutral Goldstone boson, $v \approx 246\,\text{GeV}$ is the (real and positive) vacuum expectation value (VEV), and $S_2^+, \ldots, S_n^+$ are physical charged scalars with masses $m_{C2}, \ldots, m_{Cn}$, respectively. Without loss of generality, we order the doublets Φ_k through $m_{C2} \leq m_{C3} \leq \cdots \leq m_{Cn}$. We are free to rephase each of the Φ_k, thereby mixing R_k and I_k through a 2×2 orthogonal matrix.

The real fields H, R_k, and I_k ($k = 2, \ldots, n$) are not eigenstates of mass, rather

$$\begin{pmatrix} H + iS_1^0 \\ R_2 + iI_2 \\ \vdots \\ R_n + iI_n \end{pmatrix} = \mathcal{V} \begin{pmatrix} S_1^0 \\ S_2^0 \\ \vdots \\ S_{2n}^0 \end{pmatrix}, \tag{2.2}$$

where $\mathcal{V}$ is an $n \times 2n$ matrix with (1, 1) matrix element $\mathcal{V}_{11} = i$. The physical neutral-scalar fields $S_2^0, \ldots, S_{2n}^0$ are real and have masses $m_2, \ldots, m_{2n}$, respectively. An important property of $\mathcal{V}$ is that

$$\begin{pmatrix} \mathcal{R} \\ \mathcal{I} \end{pmatrix} := \begin{pmatrix} \text{Re}\,\mathcal{V} \\ \text{Im}\,\mathcal{V} \end{pmatrix} \text{ is a } 2n \times 2n \text{ real orthogonal matrix.} \tag{2.3}$$

For the sake of simplicity, we assume alignment. This means that $H \equiv S_2^0$ is a physical neutral scalar that does *not* mix with the R_k and I_k. Hence, $\mathcal{V}_{12} = 1$ and $\mathcal{V}_{1j} = 0$, $\forall j = 3, \ldots, 2n$; also, $\mathcal{V}_{k1} = \mathcal{V}_{k2} = 0$, $\forall k = 2, \ldots, n$. The scalar H is assumed to be the particle with mass $m_2 \approx 125\,\text{GeV}$ that has been observed at the LHC. In this paper, alignment is just a simplifying assumption that we do not pretend to justify through any symmetry imposed on the nHDM. We order the S_j^0 through $m_3 \leq m_4 \leq \ldots \leq m_{2n}$. Notice that, in principle, one or more of these masses may be lower than m_2.

We define the real antisymmetric matrix

$$\mathcal{A} := \text{Im}\left(\mathcal{V}^\dagger \mathcal{V}\right) = \mathcal{R}^T \mathcal{I} - \mathcal{I}^T \mathcal{R} = \begin{pmatrix} 0 & -1 & 0 & 0 & 0 & \ldots & 0 \\ 1 & 0 & 0 & 0 & 0 & \ldots & 0 \\ 0 & 0 & 0 & \mathcal{A}_{34} & \mathcal{A}_{35} & \ldots & \mathcal{A}_{3,2n} \\ 0 & 0 & -\mathcal{A}_{34} & 0 & \mathcal{A}_{45} & \ldots & \mathcal{A}_{4,2n} \\ \vdots & \vdots & \vdots & \vdots & \vdots & \vdots & \vdots \end{pmatrix}. \tag{2.4}$$

To compute the one-loop corrections to the $Zb\bar{b}$ vertex in the nHDM, we make the simplifying assumption that only the top and bottom quarks exist and the (t, b) Cabibbo-Kobayashi-Maskawa matrix element is 1. The relevant part of the Yukawa Lagrangian

JHEP07(2021)195

is [15]

$$\mathcal{L}_{\text{Yukawa}} = -\left(\overline{t_L}\ \overline{b_L}\right)\sum_{k=2}^{n}\left[\frac{f_k}{\sqrt{2}}\begin{pmatrix}\sqrt{2}\,S_k^+\\ R_k+iI_k\end{pmatrix}b_R+\frac{e_k}{\sqrt{2}}\begin{pmatrix}R_k-iI_k\\ -\sqrt{2}\,S_k^-\end{pmatrix}t_R\right]+\text{H.c.}, \tag{2.5}$$

where the e_k and f_k are Yukawa coupling constants.

2.2 Passarino-Veltman functions

The Passarino-Veltman function $B_1\left(r^2,m_0^2,m_1^2\right)$ is defined through

$$\int\frac{\mathrm{d}^4k}{(2\pi)^4}\,\frac{1}{k^2-m_0^2}\,\frac{1}{(k+r)^2-m_1^2}\,k^\lambda=\frac{i}{16\pi^2}\,r^\lambda\,B_1\left(r^2,m_0^2,m_1^2\right). \tag{2.6}$$

The Passarino-Veltman function $C_0\left[r_1^2,(r_1-r_2)^2,r_2^2,m_0^2,m_1^2,m_2^2\right]$ is defined through

$$\int\frac{\mathrm{d}^4k}{(2\pi)^4}\,\frac{1}{k^2-m_0^2}\,\frac{1}{(k+r_1)^2-m_1^2}\,\frac{1}{(k+r_2)^2-m_2^2}=\frac{i}{16\pi^2}\,C_0\left[r_1^2,(r_1-r_2)^2,r_2^2,m_0^2,m_1^2,m_2^2\right]. \tag{2.7}$$

The Passarino-Veltman functions C_{00}, C_{11}, C_{22}, and C_{12}, which depend on r_1^2, $(r_1-r_2)^2$, r_2^2, m_0^2, m_1^2, and m_2^2 are defined through

$$\begin{aligned}\int\frac{\mathrm{d}^4k}{(2\pi)^4}\,\frac{1}{k^2-m_0^2}\,\frac{1}{(k+r_1)^2-m_1^2}\,\frac{1}{(k+r_2)^2-m_2^2}\,k^\lambda k^\nu=\frac{i}{16\pi^2}\Big[&g^{\lambda\nu}C_{00}+r_1^\lambda r_1^\nu C_{11}+r_2^\lambda r_2^\nu C_{22}\\&+\left(r_1^\lambda r_2^\nu+r_2^\lambda r_1^\nu\right)C_{12}\Big]\\&\times\left[r_1^2,(r_1-r_2)^2,r_2^2,m_0^2,m_1^2,m_2^2\right].\end{aligned} \tag{2.8}$$

The functions $B_1\left(r^2,m_0^2,m_1^2\right)$ and $C_{00}\left[r_1^2,(r_1-r_2)^2,r_2^2,m_0^2,m_1^2,m_2^2\right]$ are divergent, yet the functions $f_{L,R}\left(m^2\right)$ and $h_{L,R}\left(m_j^2,m_{j'}^2\right)$ that are defined below in equations (2.11) and (2.14), respectively, are finite.

2.3 The charged-scalar contribution

In the nHDM at the one-loop level, both δg_L and δg_R are the sum of a contribution, which we denote through a superscript c, from diagrams having charged scalars and top quarks in the internal lines of the loop, and another contribution, which we denote through a superscript n, from diagrams with neutral scalars and bottom quarks in the internal lines:

$$\delta g_L=\delta g_L^c+\delta g_L^n,\quad \delta g_R=\delta g_R^c+\delta g_R^n. \tag{2.9}$$

The charged-scalar contribution has been computed long time ago [3]. It corresponds to the computation of the diagrams in figure 1. It is

$$\delta g_L^c=\frac{1}{16\pi^2}\sum_{k=2}^{n}\left|e_k\right|^2 f_L\left(m_{Ck}^2\right),\quad \delta g_R^c=\frac{1}{16\pi^2}\sum_{k=2}^{n}\left|f_k\right|^2 f_R\left(m_{Ck}^2\right), \tag{2.10}$$

JHEP07(2021)195

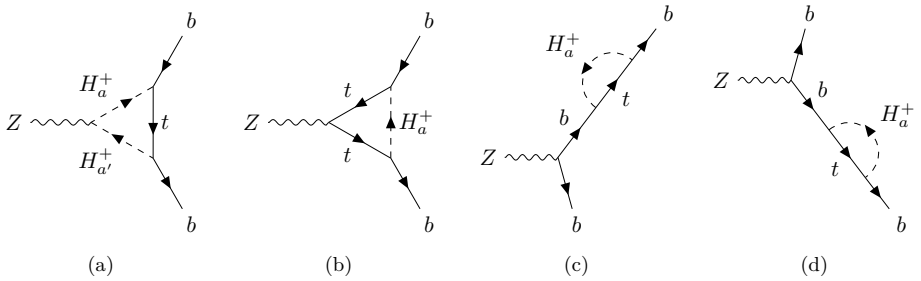

Figure 1. Feynman diagrams that produce equations (2.10) and (2.11).

where the functions f_L and f_R are defined through

$$\begin{aligned} f_L\left(m^2\right) = & \left(2s_w^2-1\right) C_{00}\left(0,\, m_Z^2,\, 0,\, m_t^2,\, m^2,\, m^2\right) \\ & + \left(\frac{2s_w^2}{3}-\frac{1}{2}\right) m_t^2\, C_0\left(0,\, m_Z^2,\, 0,\, m^2,\, m_t^2,\, m_t^2\right) \\ & - \frac{2s_w^2}{3}\left[2\, C_{00}\left(0,\, m_Z^2,\, 0,\, m^2,\, m_t^2,\, m_t^2\right) - \frac{1}{2}\right. \\ & \left. - m_Z^2\, C_{12}\left(0,\, m_Z^2,\, 0,\, m^2,\, m_t^2,\, m_t^2\right)\right] \\ & + \left(\frac{s_w^2}{3}-\frac{1}{2}\right) B_1\left(0,\, m_t^2, m^2\right), \end{aligned} \tag{2.11a}$$

$$\begin{aligned} f_R\left(m^2\right) = & \left(2s_w^2-1\right) C_{00}\left(0,\, m_Z^2,\, 0,\, m_t^2,\, m^2,\, m^2\right) \\ & + \frac{2s_w^2}{3}\, m_t^2\, C_0\left(0,\, m_Z^2,\, 0,\, m^2,\, m_t^2,\, m_t^2\right) \\ & + \left(\frac{1}{2}-\frac{2s_w^2}{3}\right)\left[2\, C_{00}\left(0,\, m_Z^2,\, 0,\, m^2,\, m_t^2,\, m_t^2\right) - \frac{1}{2}\right. \\ & \left. - m_Z^2\, C_{12}\left(0,\, m_Z^2,\, 0,\, m^2,\, m_t^2,\, m_t^2\right)\right] \\ & + \frac{s_w^2}{3}\, B_1\left(0,\, m_t^2, m^2\right). \end{aligned} \tag{2.11b}$$

In equations (2.11) m_t is the top-quark mass and m_Z is the mass of the gauge boson Z^0. In the approximation $m_Z = 0$, the functions f_L and f_R do not depend of s_w,[3] and are symmetric of each other:

$$f_R\left(m^2\right) \approx -f_L\left(m^2\right) \approx \frac{1}{2}\,\frac{x}{1-x}\left(1+\frac{\ln x}{1-x}\right), \tag{2.12}$$

where $x = m_t^2/m^2$. Remarkably, the approximations (2.12) hold very well even when one computes f_L and f_R with $m_Z = 91.1876\,\text{GeV}$. The functions f_L and f_R are depicted in figure 2.[4] One sees that $f_L\left(m^2\right) > 0$, $f_R\left(m^2\right) < 0$, and $f_R\left(m^2\right) \approx -f_L\left(m^2\right)$ for all

[3]When $m_Z = 0$ the Z^0 is indistinguishable from the photon and therefore the weak mixing angle is arbitrary and unphysical.

[4]We have performed the numerical computation of Passarino-Veltman functions by using the Fortran library Collier [16] through interface CollierLink [17].

JHEP07(2021)195

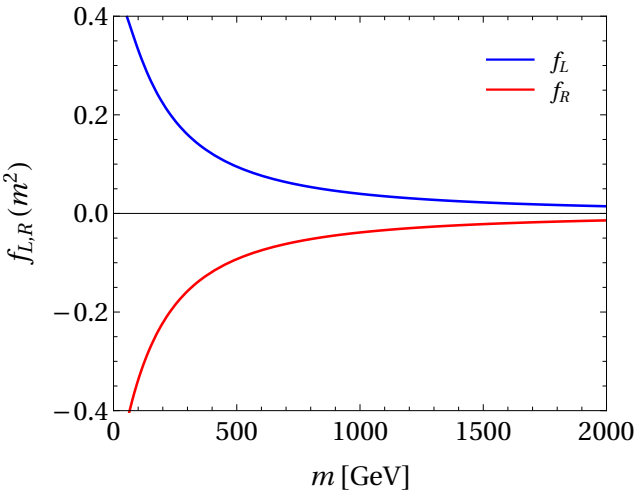

Figure 2. The functions $f_L\left(m^2\right)$ and $f_R\left(m^2\right)$.

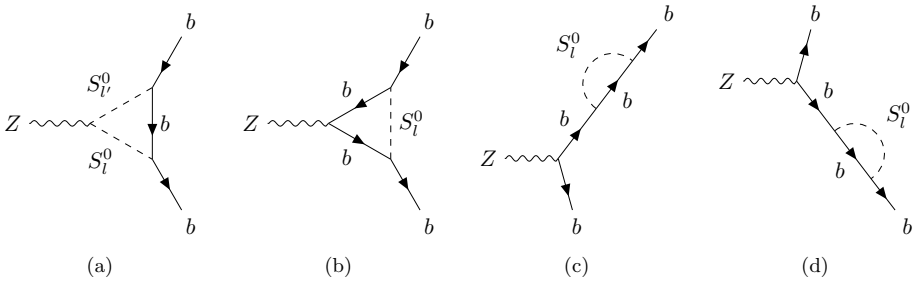

Figure 3. Feynman diagrams that produce equations (2.13) and (2.14).

values of m^2. Moreover, the absolute values of both functions decrease with increasing m^2. Therefore, $\delta g_L^c > 0$, $\delta g_R^c < 0$, and both δg_L^c and $-\delta g_R^c$ are monotonically decreasing functions of the charged-scalar masses.

2.4 The neutral-scalar contribution

The neutral-scalar contribution to δg_L and δg_R has been recently emphasized in ref. [15], following the original computation in ref. [3]; it corresponds to the computation of the diagrams in figure 3 and it is recapitulated in appendix B.[5] Assuming alignment and discarding the Standard-Model contributions that involve S_1^0 and S_2^0, one has

$$\delta g_L^n = \frac{1}{16\pi^2} \sum_{j=3}^{2n-1} \sum_{j'=j+1}^{2n} \mathcal{A}_{jj'}\, \mathrm{Im}\left[\left(\mathcal{V}^\dagger \mathcal{F}^*\right)_j \left(\mathcal{V}^T \mathcal{F}\right)_{j'}\right] h_L\left(m_j^2,\, m_{j'}^2\right), \tag{2.13a}$$

$$\delta g_R^n = \frac{1}{16\pi^2} \sum_{j=3}^{2n-1} \sum_{j'=j+1}^{2n} \mathcal{A}_{jj'}\, \mathrm{Im}\left[\left(\mathcal{V}^\dagger \mathcal{F}^*\right)_j \left(\mathcal{V}^T \mathcal{F}\right)_{j'}\right] h_R\left(m_j^2,\, m_{j'}^2\right), \tag{2.13b}$$

[5] The diagrams in figure 4 do not contribute to δg_L and δg_R in our case. This is so because diagrams (a) and (b) only exist, if there are only scalar doublets, when H_a^+ is the charged Goldstone boson, and because diagrams (c) and (d) are proportional to the bottom-quark mass.

JHEP07(2021)195

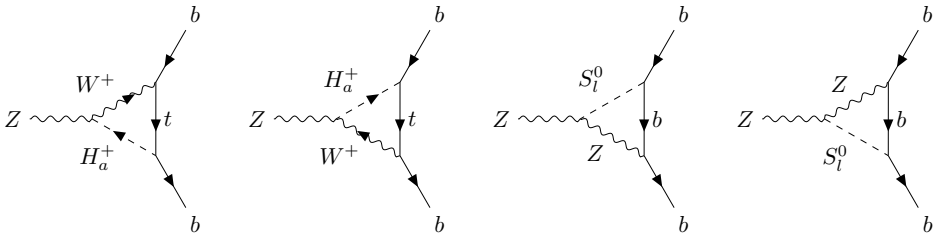

Figure 4. Feynman diagrams that do not contribute to δg_L and δg_R in the specific case of this paper.

where $\mathcal{F}$ is an $n \times 1$ vector with k^{th} component $\mathcal{F}_k = f_k$ for $k = 2, \ldots, n$, and

$$\begin{aligned} h_L\left(m_j^2,\, m_{j'}^2\right) = & -C_{00}\left(0,\, m_Z^2,\, 0,\, 0,\, m_j^2,\, m_{j'}^2\right) \\ & + \frac{s_w^2}{6}\left[2\,C_{00}\left(0,\, m_Z^2,\, 0,\, m_j^2,\, 0,\, 0\right) + 2\,C_{00}\left(0,\, m_Z^2,\, 0,\, m_{j'}^2,\, 0,\, 0\right)\right. \\ & \left. -1 - m_Z^2\,C_{12}\left(0,\, m_Z^2,\, 0,\, m_j^2,\, 0,\, 0\right) - m_Z^2\,C_{12}\left(0,\, m_Z^2,\, 0,\, m_{j'}^2,\, 0,\, 0\right)\right] \\ & + \left(\frac{s_w^2}{6} - \frac{1}{4}\right)\left[B_1\left(0,\, 0,\, m_j^2\right) + B_1\left(0,\, 0,\, m_{j'}^2\right)\right], \end{aligned} \tag{2.14a}$$

$$\begin{aligned} h_R\left(m_j^2,\, m_{j'}^2\right) = & \; C_{00}\left(0,\, m_Z^2,\, 0,\, 0,\, m_j^2,\, m_{j'}^2\right) \\ & + \left(\frac{s_w^2}{6} - \frac{1}{4}\right)\left[2\,C_{00}\left(0,\, m_Z^2,\, 0,\, m_j^2,\, 0,\, 0\right) + 2\,C_{00}\left(0,\, m_Z^2,\, 0,\, m_{j'}^2,\, 0,\, 0\right)\right. \\ & \left. -1 - m_Z^2\,C_{12}\left(0,\, m_Z^2,\, 0,\, m_j^2,\, 0,\, 0\right) - m_Z^2\,C_{12}\left(0,\, m_Z^2,\, 0,\, m_{j'}^2,\, 0,\, 0\right)\right] \\ & + \frac{s_w^2}{6}\left[B_1\left(0,\, 0,\, m_j^2\right) + B_1\left(0,\, 0,\, m_{j'}^2\right)\right]. \end{aligned} \tag{2.14b}$$

The functions h_L and h_R are independent of s_w when $m_Z = 0$; however, that approximation is not a good one for those functions. We depict their real parts in figure 5.[6] One sees that, when both m_j and $m_{j'}$ are larger than the Fermi scale, $h_L\left(m_j^2,\, m_{j'}^2\right) > 0$ and $h_R\left(m_j^2,\, m_{j'}^2\right) < 0$. However, if both $m_j \lesssim 100\,\text{GeV}$ and $m_{j'} \lesssim 100\,\text{GeV}$, then both $h_L\left(m_j^2,\, m_{j'}^2\right)$ and $h_R\left(m_j^2,\, m_{j'}^2\right)$ invert their usual signs. Moreover, $\left|h_L\left(m_j^2,\, m_{j'}^2\right)\right|$ and $\left|h_R\left(m_j^2,\, m_{j'}^2\right)\right|$ become rather large either when $|m_j - m_{j'}| \gtrsim 200\,\text{GeV}$ and one of the masses $\lesssim 50\,\text{GeV}$, or when both m_j and $m_{j'} \lesssim 50\,\text{GeV}$.

[6] The functions h_L and h_R are complex. However, their imaginary parts are irrelevant for the computation of g_L and g_R, since they do not interfere with the tree-level contributions to those parameters [15], which are real. Therefore, in this paper whenever we talk about h_L and h_R we really mean just the real parts of those two functions.

JHEP07(2021)195

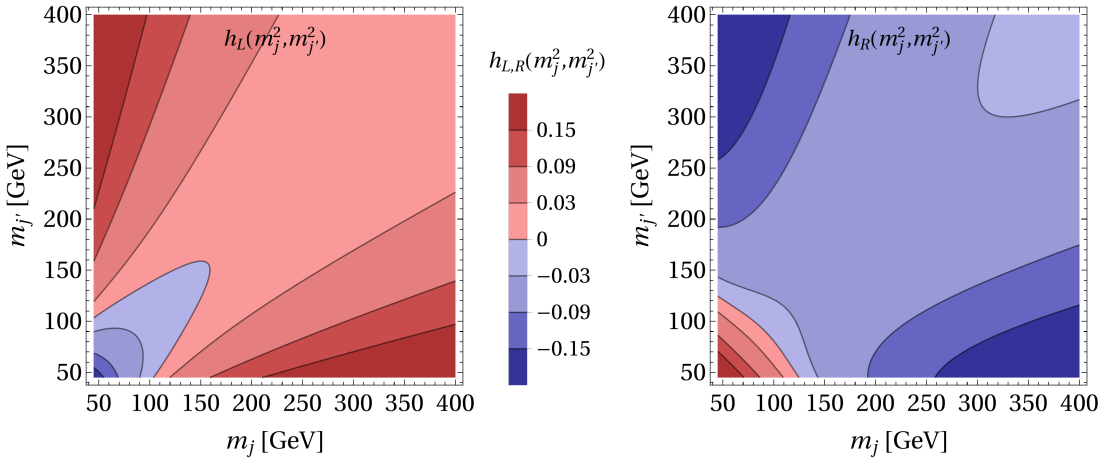

Figure 5. The functions $h_L\left(m_j^2,\, m_{j'}^2\right)$ and $h_R\left(m_j^2,\, m_{j'}^2\right)$.

3 The aligned 2HDM

In a two-Higgs-doublet model with alignment [15], the doublet Φ_2 may be rephased so that $R_2 \equiv S_3^0$ and $I_2 \equiv S_4^0$ are the new physical neutral scalars. Then,

$$\mathcal{V} = \begin{pmatrix} i & 1 & 0 & 0 \\ 0 & 0 & 1 & i \end{pmatrix}, \tag{3.1}$$

hence $\mathcal{A}_{34} = 1$ and $\left(\mathcal{V}^\dagger \mathcal{F}^*\right)_3 \left(\mathcal{V}^T \mathcal{F}\right)_4 = i\,|f_2|^2$. There are five New-Physics parameters on which δg_L and δg_R depend: the neutral-scalar masses m_3 and m_4, the charged-scalar mass m_{C2}, and the Yukawa couplings e_2 and f_2. One has [15]

$$\delta g_L = \frac{|e_2|^2\, f_L\left(m_{C2}^2\right) + |f_2|^2\, h_L\left(m_3^2,\, m_4^2\right)}{16\pi^2}, \tag{3.2a}$$

$$\delta g_R = \frac{|f_2|^2 \left[f_R\left(m_{C2}^2\right) + h_R\left(m_3^2,\, m_4^2\right)\right]}{16\pi^2}. \tag{3.2b}$$

We now consider the scalar potential of the 2HDM [18],

$$\begin{aligned} V \,=\, & \mu_1\, \Phi_1^\dagger \Phi_1 + \mu_2\, \Phi_2^\dagger \Phi_2 + \left(\mu_3\, \Phi_1^\dagger \Phi_2 + \text{H.c.}\right) \\ & + \frac{\lambda_1}{2} \left(\Phi_1^\dagger \Phi_1\right)^2 + \frac{\lambda_2}{2} \left(\Phi_2^\dagger \Phi_2\right)^2 + \lambda_3\, \Phi_1^\dagger \Phi_1\, \Phi_2^\dagger \Phi_2 + \lambda_4\, \Phi_1^\dagger \Phi_2\, \Phi_2^\dagger \Phi_1 \\ & + \left[\frac{\lambda_5}{2} \left(\Phi_1^\dagger \Phi_2\right)^2 + \lambda_6\, \Phi_1^\dagger \Phi_1\, \Phi_1^\dagger \Phi_2 + \lambda_7\, \Phi_2^\dagger \Phi_2\, \Phi_1^\dagger \Phi_2 + \text{H.c.}\right]. \end{aligned} \tag{3.3}$$

In the Higgs basis, $\mu_1 = -\,\lambda_1 v^2/\,2$ and $\mu_3 = -\,\lambda_6 v^2/\,2$. Because of alignment, λ_6 (and μ_3) are zero and

$$\lambda_1 = \frac{m_2^2}{v^2} = \left(\frac{125\,\text{GeV}}{246\,\text{GeV}}\right)^2 \approx 0.258. \tag{3.4}$$

From the masses of the scalars we compute

$$\lambda_4 = \frac{m_3^2 + m_4^2 - 2m_{C2}^2}{v^2}, \quad \Lambda_5 = \frac{m_4^2 - m_3^2}{v^2}, \tag{3.5}$$

where $\Lambda_5 := |\lambda_5|$.

JHEP07(2021)195

The masses m_{C2}, m_3, and m_4 are not completely free, because they must comply with unitarity (UNI) and bounded-from-below (BFB) requirements [18]. For the sake of simplicity, in our analysis we assume $\lambda_2 = \lambda_7 = 0$. We enforce the UNI conditions

$$\lambda_4^2 < 64\pi^2 - 8\pi\lambda_1, \quad \Lambda_5^2 < 64\pi^2 - 8\pi\lambda_1 \tag{3.6}$$

on the quantities (3.5). Additionally, there are

- BFB conditions [18]

$$\lambda_3 > 0, \quad \lambda_3 + \lambda_4 - \Lambda_5 > 0; \tag{3.7}$$

- UNI conditions [18]

$$\begin{aligned} |\lambda_3| + |\lambda_4| &< 8\pi, \qquad |\lambda_3| + \Lambda_5 < 8\pi, \\ |\lambda_3 + 2\lambda_4| + 3\Lambda_5 &< 8\pi, \quad (2\lambda_3 + \lambda_4)^2 < 64\pi^2 - 24\pi\lambda_1; \end{aligned} \tag{3.8}$$

- the condition to avoid the situation of 'panic vacuum', namely [19–22]

$$\left[\left(\frac{m_{C2}^2}{v^2} + \frac{\lambda_4}{2}\right)^2 - \frac{\Lambda_5^2}{4}\right]\left(\frac{m_{C2}^2}{v^2} - \frac{\lambda_3}{2}\right) > 0. \tag{3.9}$$

After computing λ_4 and Λ_5 through equations (3.5) and after checking inequalities (3.6), we verify whether there is any value of λ_3 that satisfies the inequalities (3.7)–(3.9); if there is, then the inputed masses m_{C2}, m_3, and m_4 are valid; else, they are not.

We also compute the contribution of the new scalars to the oblique parameter

$$T = \frac{1}{16\pi s_w^2 m_W^2}\left[F\left(m_{C2}^2,\ m_3^2\right) + F\left(m_{C2}^2,\ m_4^2\right) - F\left(m_3^2,\ m_4^2\right)\right], \tag{3.10}$$

where $m_W = 80.4\,\text{GeV}$ is the mass of the gauge bosons $W^\pm$ and

$$F(A,\,B) = \begin{cases} \dfrac{A+B}{2} - \dfrac{AB}{A-B}\ln\dfrac{A}{B} & \Leftarrow A \neq B, \\ 0 & \Leftarrow A = B. \end{cases} \tag{3.11}$$

Additionally, we apply constraints on the oblique parameter [23–26]

$$S = \frac{4s_w^2 c_w^2}{\alpha}\left[\left.\frac{\partial A_{ZZ}(q^2)}{\partial q^2}\right|_{q^2=m_Z^2} - \left.\frac{\partial A_{\gamma\gamma}(q^2)}{\partial q^2}\right|_{q^2=0} + \frac{c_w^2 - s_w^2}{c_w s_w}\left.\frac{\partial A_{\gamma Z}(q^2)}{\partial q^2}\right|_{q^2=0}\right]. \tag{3.12}$$

This parameter has been computed in ref. [27] to be

$$S = \frac{1}{24\pi}\left[\ln\frac{m_3^2 m_4^2}{m_{C2}^4} + \left(s_w^2 - c_w^2\right)^2 f\left(m_{C2}^2,\, m_{C2}^2,\, m_Z^2\right) + f\left(m_3^2,\, m_4^2,\, m_Z^2\right)\right]. \tag{3.13}$$

Here,

$$f(A,\,B,\,C) = -\frac{10}{3} - 4\frac{A+B}{C} + 4\frac{(A-B)^2}{C^2} + \left[3\frac{A^2-B^2}{C^2} - 2\frac{(A-B)^3}{C^3}\right]\ln\frac{A}{B} \tag{3.14a}$$

$$+\left[\frac{1}{C} + \frac{A+B}{C^2} - 2\frac{(A-B)^2}{C^3}\right]h(t,\,r), \tag{3.14b}$$

JHEP07(2021)195

where $t \equiv A + B - C$, $r \equiv A^2 + B^2 + C^2 - 2\,(AB + AC + BC)$, and

$$h\,(t,\,r) = \begin{cases} \sqrt{r}\,\ln\left|\dfrac{t-\sqrt{r}}{t+\sqrt{r}}\right| & \Leftarrow r > 0, \\ 0 & \Leftarrow r = 0, \\ 2\,\sqrt{-r}\,\arctan\dfrac{\sqrt{-r}}{t} & \Leftarrow r < 0. \end{cases} \tag{3.15}$$

We either enforce the phenomenological constraint [1]

$$T = 0.03 \pm 0.12, \tag{3.16a}$$
$$S = -0.01 \pm 0.10 \tag{3.16b}$$

or we allow for other New Physics beyond the 2HDM and apply milder requirements by allowing values of T and S within its 3σ and 2σ bounds, respectively.

4 The aligned 3HDM

4.1 Parameterization of the neutral-scalar mixing

In the three-Higgs-doublet model with alignment,

$$\begin{pmatrix} R_2 \\ R_3 \\ I_2 \\ I_3 \end{pmatrix} = \mathcal{T} \begin{pmatrix} S_3^0 \\ S_4^0 \\ S_5^0 \\ S_6^0 \end{pmatrix}, \tag{4.1}$$

where $\mathcal{T}$ is a 4×4 real orthogonal matrix. We parameterize

$$\mathcal{T} = \mathcal{O}_{13}\,(\theta_5) \times \mathcal{O}_{24}\,(\theta_6) \times \mathcal{O}_{12}\,(\theta_1) \times \mathcal{O}_{34}\,(\theta_2) \times \mathcal{O}_{14}\,(\theta_3) \times \mathcal{O}_{23}\,(\theta_4)\,, \tag{4.2}$$

where $\mathcal{O}_{pq}\,(\theta)$ represents a rotation through an angle θ in the $(p,\,q)$ plane. Now, $\mathcal{O}_{13}\,(\theta_5)$ is a rotation that mixes R_2 and I_2, and $\mathcal{O}_{24}\,(\theta_6)$ is a rotation mixing R_3 and I_3, viz. they represent rephasings of the doublets Φ_2 and Φ_3, respectively. Since such rephasings are unphysical, one may without loss of generality drop those two rotations from the parameterization (4.2), obtaining

$$\mathcal{T} = \begin{pmatrix} c_1c_3 & -s_1c_4 & s_1s_4 & -c_1s_3 \\ s_1c_3 & c_1c_4 & -c_1s_4 & -s_1s_3 \\ -s_2s_3 & c_2s_4 & c_2c_4 & -s_2c_3 \\ c_2s_3 & s_2s_4 & s_2c_4 & c_2c_3 \end{pmatrix}, \tag{4.3}$$

JHEP07(2021)195

where $c_p = \cos\theta_p$ and $s_p = \sin\theta_p$ for $p = 1, 2, 3, 4$. Then,

$$\delta g_L = \frac{|e_2|^2 f_L\left(m_{C2}^2\right) + |e_3|^2 f_L\left(m_{C3}^2\right)}{16\pi^2} + \frac{1}{16\pi^2}\sum_{j=3}^{5}\sum_{j'=j+1}^{6}\mathcal{A}_{jj'}\,\mathrm{Im}\left[\left(\mathcal{V}^\dagger\mathcal{F}^*\right)_j\left(\mathcal{V}^T\mathcal{F}\right)_{j'}\right] h_L\left(m_j^2, m_{j'}^2\right), \tag{4.4a}$$

$$\delta g_R = \frac{|f_2|^2 f_R\left(m_{C2}^2\right) + |f_3|^2 f_R\left(m_{C3}^2\right)}{16\pi^2} + \frac{1}{16\pi^2}\sum_{j=3}^{5}\sum_{j'=j+1}^{6}\mathcal{A}_{jj'}\,\mathrm{Im}\left[\left(\mathcal{V}^\dagger\mathcal{F}^*\right)_j\left(\mathcal{V}^T\mathcal{F}\right)_{j'}\right] h_R\left(m_j^2, m_{j'}^2\right), \tag{4.4b}$$

with

$$\mathcal{A}_{34} = -\mathcal{A}_{56} = (c_1c_2 + s_1s_2)(c_3s_4 - s_3c_4), \tag{4.5a}$$
$$\mathcal{A}_{35} = \mathcal{A}_{46} = (c_1c_2 + s_1s_2)(c_3c_4 + s_3s_4), \tag{4.5b}$$
$$\mathcal{A}_{36} = -\mathcal{A}_{45} = s_1c_2 - c_1s_2, \tag{4.5c}$$

and

$$\begin{aligned}\mathrm{Im}\left[\left(\mathcal{V}^\dagger\mathcal{F}^*\right)_3\left(\mathcal{V}^T\mathcal{F}\right)_4\right] &= |f_2|^2(c_1c_2c_3s_4 - s_1s_2s_3c_4) + |f_3|^2(s_1s_2c_3s_4 - c_1c_2s_3c_4)\\ &\quad + \mathrm{Re}\left(f_2f_3^*\right)(c_1s_2 + s_1c_2)(c_3s_4 + s_3c_4)\\ &\quad + \mathrm{Im}\left(f_2f_3^*\right)(s_3s_4 - c_3c_4),\end{aligned} \tag{4.6a}$$

$$\begin{aligned}\mathrm{Im}\left[\left(\mathcal{V}^\dagger\mathcal{F}^*\right)_3\left(\mathcal{V}^T\mathcal{F}\right)_5\right] &= |f_2|^2(c_1c_2c_3c_4 + s_1s_2s_3s_4) + |f_3|^2(s_1s_2c_3c_4 + c_1c_2s_3s_4)\\ &\quad + \mathrm{Re}\left(f_2f_3^*\right)(c_1s_2 + s_1c_2)(c_3c_4 - s_3s_4)\\ &\quad + \mathrm{Im}\left(f_2f_3^*\right)(c_3s_4 + s_3c_4),\end{aligned} \tag{4.6b}$$

$$\mathrm{Im}\left[\left(\mathcal{V}^\dagger\mathcal{F}^*\right)_3\left(\mathcal{V}^T\mathcal{F}\right)_6\right] = -c_1s_2\,|f_2|^2 + s_1c_2\,|f_3|^2 + \mathrm{Re}\left(f_2f_3^*\right)(c_1c_2 - s_1s_2), \tag{4.6c}$$

$$\mathrm{Im}\left[\left(\mathcal{V}^\dagger\mathcal{F}^*\right)_4\left(\mathcal{V}^T\mathcal{F}\right)_5\right] = -s_1c_2\,|f_2|^2 + c_1s_2\,|f_3|^2 + \mathrm{Re}\left(f_2f_3^*\right)(c_1c_2 - s_1s_2), \tag{4.6d}$$

$$\begin{aligned}\mathrm{Im}\left[\left(\mathcal{V}^\dagger\mathcal{F}^*\right)_4\left(\mathcal{V}^T\mathcal{F}\right)_6\right] &= |f_2|^2(s_1s_2c_3c_4 + c_1c_2s_3s_4) + |f_3|^2(c_1c_2c_3c_4 + s_1s_2s_3s_4)\\ &\quad - \mathrm{Re}\left(f_2f_3^*\right)(c_1s_2 + s_1c_2)(c_3c_4 - s_3s_4),\\ &\quad - \mathrm{Im}\left(f_2f_3^*\right)(c_3s_4 + s_3c_4),\end{aligned} \tag{4.6e}$$

$$\begin{aligned}\mathrm{Im}\left[\left(\mathcal{V}^\dagger\mathcal{F}^*\right)_5\left(\mathcal{V}^T\mathcal{F}\right)_6\right] &= |f_2|^2(c_1c_2s_3c_4 - s_1s_2c_3s_4) + |f_3|^2(s_1s_2s_3c_4 - c_1c_2c_3s_4)\\ &\quad + \mathrm{Re}\left(f_2f_3^*\right)(c_1s_2 + s_1c_2)(c_3s_4 + s_3c_4),\\ &\quad + \mathrm{Im}\left(f_2f_3^*\right)(s_3s_4 - c_3c_4).\end{aligned} \tag{4.6f}$$

The contribution of the new scalars to the oblique parameter T, given in equation (23)

JHEP07(2021)195

of ref. [28], is

$$
\begin{aligned}
T = \frac{1}{16\pi s_w^2 m_W^2} \Big\{ & \left(c_1^2 c_3^2 + s_2^2 s_3^2\right) F\left(m_{C2}^2,\, m_3^2\right) + \left(s_1^2 c_4^2 + c_2^2 s_4^2\right) F\left(m_{C2}^2,\, m_4^2\right) \\
& + \left(s_1^2 s_4^2 + c_2^2 c_4^2\right) F\left(m_{C2}^2,\, m_5^2\right) + \left(c_1^2 s_3^2 + s_2^2 c_3^2\right) F\left(m_{C2}^2,\, m_6^2\right) \\
& + \left(s_1^2 c_3^2 + c_2^2 s_3^2\right) F\left(m_{C3}^2,\, m_3^2\right) + \left(c_1^2 c_4^2 + s_2^2 s_4^2\right) F\left(m_{C3}^2,\, m_4^2\right) \\
& + \left(c_1^2 s_4^2 + s_2^2 c_4^2\right) F\left(m_{C3}^2,\, m_5^2\right) + \left(s_1^2 s_3^2 + c_2^2 c_3^2\right) F\left(m_{C3}^2,\, m_6^2\right) \\
& - \left(\mathcal{A}_{34}\right)^2 \left[F\left(m_3^2,\, m_4^2\right) + F\left(m_5^2,\, m_6^2\right)\right] \\
& - \left(\mathcal{A}_{35}\right)^2 \left[F\left(m_3^2,\, m_5^2\right) + F\left(m_4^2,\, m_6^2\right)\right] \\
& - \left(\mathcal{A}_{36}\right)^2 \left[F\left(m_3^2,\, m_6^2\right) + F\left(m_4^2,\, m_5^2\right)\right] \Big\} .
\end{aligned}
\tag{4.7}
$$

For the oblique parameter S one has

$$
\begin{aligned}
S = \frac{1}{24\pi} \Big\{ & \left(s_w^2 - c_w^2\right)^2 \left[f\left(m_{C2}^2,\, m_{C2}^2,\, m_Z^2\right) + f\left(m_{C3}^2,\, m_{C3}^2,\, m_Z^2\right)\right] && \text{(4.8a)} \\
& + \ln \frac{m_3^2 m_4^2 m_5^2 m_6^2}{m_{C2}^4 m_{C3}^4} + \left(\mathcal{A}_{34}\right)^2 \left[f\left(m_3^2,\, m_4^2,\, m_Z^2\right) + f\left(m_5^2,\, m_6^2,\, m_Z^2\right)\right] && \text{(4.8b)} \\
& + \left(\mathcal{A}_{35}\right)^2 \left[f\left(m_3^2,\, m_5^2,\, m_Z^2\right) + f\left(m_4^2,\, m_6^2,\, m_Z^2\right)\right] && \text{(4.8c)} \\
& + \left(\mathcal{A}_{45}\right)^2 \left[f\left(m_3^2,\, m_6^2,\, m_Z^2\right) + f\left(m_4^2,\, m_5^2,\, m_Z^2\right)\right] \Big\} . && \text{(4.8d)}
\end{aligned}
$$

4.2 The scalar potential

The parameters The scalar potential of the 3HDM has lots of couplings and it is impractical to work with it. So we concentrate on a truncated version of the potential, viz. we discard from the quartic part of the potential all the terms that either do not contain Φ_1 or are linear in Φ_1.[7] The remaining potential is

$$
\begin{aligned}
V = & \, \mu_1 \, \Phi_1^\dagger \Phi_1 + \mu_2 \, \Phi_2^\dagger \Phi_2 + \mu_3 \, \Phi_3^\dagger \Phi_3 + \left(\mu_4 \, \Phi_1^\dagger \Phi_2 + \mu_5 \, \Phi_1^\dagger \Phi_3 + \mu_6 \, \Phi_2^\dagger \Phi_3 + \text{H.c.}\right) \\
& + \frac{\lambda_1}{2} \left(\Phi_1^\dagger \Phi_1\right)^2 + \lambda_4 \, \Phi_1^\dagger \Phi_1 \, \Phi_2^\dagger \Phi_2 + \lambda_5 \, \Phi_1^\dagger \Phi_1 \, \Phi_3^\dagger \Phi_3 + \lambda_7 \, \Phi_1^\dagger \Phi_2 \, \Phi_2^\dagger \Phi_1 + \lambda_8 \, \Phi_1^\dagger \Phi_3 \, \Phi_3^\dagger \Phi_1 \\
& + \left[\frac{\lambda_{10}}{2} \left(\Phi_1^\dagger \Phi_2\right)^2 + \frac{\lambda_{11}}{2} \left(\Phi_1^\dagger \Phi_3\right)^2 + \lambda_{13} \, \Phi_1^\dagger \Phi_1 \, \Phi_1^\dagger \Phi_2 + \lambda_{14} \, \Phi_1^\dagger \Phi_1 \, \Phi_1^\dagger \Phi_3 \right. \\
& \left. + \lambda_{19} \, \Phi_1^\dagger \Phi_1 \, \Phi_2^\dagger \Phi_3 + \lambda_{22} \, \Phi_1^\dagger \Phi_3 \, \Phi_2^\dagger \Phi_1 + \lambda_{25} \, \Phi_1^\dagger \Phi_2 \, \Phi_1^\dagger \Phi_3 + \text{H.c.}\right] ,
\end{aligned}
\tag{4.9}
$$

where $\mu_{1,2,3}$ and $\lambda_{1,4,5,7,8}$ are real and the remaining parameters are in general complex. In order that the VEV of Φ_1 is $v \Big/ \sqrt{2}$ and the VEVs of Φ_2 and Φ_3 are zero, one must have

$$
\mu_1 = -\frac{\lambda_1 v^2}{2}, \quad \mu_4 = -\frac{\lambda_{13} v^2}{2}, \quad \mu_5 = -\frac{\lambda_{14} v^2}{2}. \tag{4.10}
$$

[7] This is equivalent to discarding from the scalar potential of the 2HDM the terms with coefficients λ_2 and λ_7, like we did in the previous section.

JHEP07(2021)195

In order that the charged-scalar mass matrix is diag (m_{C2}^2, m_{C3}^2), one must have

$$\mu_2 = m_{C2}^2 - \frac{\lambda_4 v^2}{2}, \quad \mu_3 = m_{C3}^2 - \frac{\lambda_5 v^2}{2}, \quad \mu_6 = -\frac{\lambda_{19} v^2}{2}. \tag{4.11}$$

Equations (4.10) and (4.11) are the conditions for the charged Higgs basis. Next we write down the conditions for alignment, i.e. for $H \equiv S_2^0$ to have mass m_2 and not to have mass terms together with either R_2, R_3, I_2, or I_3:

$$\lambda_1 = \frac{m_2^2}{v^2} \approx 0.258, \quad \lambda_{13} = \lambda_{14} = 0, \tag{4.12}$$

hence μ_4 and μ_5 are zero too. The mass terms of R_2, R_3, I_2, and I_3 are given by

$$V = \cdots + \frac{1}{2} \begin{pmatrix} R_2, & R_3, & I_2, & I_3 \end{pmatrix} N \begin{pmatrix} R_2 \\ R_3 \\ I_2 \\ I_3 \end{pmatrix}, \tag{4.13}$$

where N is a 4×4 real symmetric matrix. Using equations (4.1) and (4.3), one finds that

$$N_{11} - m_{C2}^2 =$$
$$\frac{v^2}{2}(\lambda_7 + \operatorname{Re}\lambda_{10}) = m_3^2 c_1^2 c_3^2 + m_4^4 s_1^2 c_3^2 + m_5^2 s_2^2 s_3^2 + m_6^2 c_2^2 s_3^2 - m_{C2}^2, \tag{4.14a}$$
$$N_{33} - m_{C2}^2 =$$
$$\frac{v^2}{2}(\lambda_7 - \operatorname{Re}\lambda_{10}) = m_3^2 s_1^2 s_4^2 + m_4^4 c_1^2 s_4^2 + m_5^2 c_2^2 c_4^2 + m_6^2 s_2^2 c_4^2 - m_{C2}^2, \tag{4.14b}$$
$$N_{13} = -\frac{v^2}{2}\operatorname{Im}\lambda_{10} = \left(m_3^2 - m_4^2\right) c_1 s_1 c_3 s_4 + \left(m_6^2 - m_5^2\right) c_2 s_2 s_3 c_4, \tag{4.14c}$$
$$N_{22} - m_{C3}^2 =$$
$$\frac{v^2}{2}(\lambda_8 + \operatorname{Re}\lambda_{11}) = m_3^2 s_1^2 c_4^2 + m_4^4 c_1^2 c_4^2 + m_5^2 c_2^2 s_4^2 + m_6^2 s_2^2 s_4^2 - m_{C3}^2, \tag{4.14d}$$
$$N_{44} - m_{C3}^2 =$$
$$\frac{v^2}{2}(\lambda_8 - \operatorname{Re}\lambda_{11}) = m_3^2 c_1^2 s_3^2 + m_4^4 s_1^2 s_3^2 + m_5^2 s_2^2 c_3^2 + m_6^2 c_2^2 c_3^2 - m_{C3}^2, \tag{4.14e}$$
$$N_{24} = -\frac{v^2}{2}\operatorname{Im}\lambda_{11} = \left(m_3^2 - m_4^2\right) c_1 s_1 s_3 c_4 + \left(m_6^2 - m_5^2\right) c_2 s_2 c_3 s_4, \tag{4.14f}$$
$$N_{12} = \frac{v^2}{2}\operatorname{Re}(\lambda_{22} + \lambda_{25}) = \left(m_4^2 - m_3^2\right) c_1 s_1 c_3 c_4 + \left(m_6^2 - m_5^2\right) c_2 s_2 s_3 s_4, \tag{4.14g}$$
$$N_{34} = \frac{v^2}{2}\operatorname{Re}(\lambda_{22} - \lambda_{25}) = \left(m_4^2 - m_3^2\right) c_1 s_1 s_3 s_4 + \left(m_6^2 - m_5^2\right) c_2 s_2 c_3 c_4, \tag{4.14h}$$
$$N_{14} = -\frac{v^2}{2}\operatorname{Im}(\lambda_{22} + \lambda_{25}) = c_3 s_3 \left(-c_1^2 m_3^2 - s_1^2 m_4^2 + s_2^2 m_5^2 + c_2^2 m_6^2\right), \tag{4.14i}$$
$$N_{23} = \frac{v^2}{2}\operatorname{Im}(\lambda_{22} - \lambda_{25}) = c_4 s_4 \left(-s_1^2 m_3^2 - c_1^2 m_4^2 + c_2^2 m_5^2 + s_2^2 m_6^2\right). \tag{4.14j}$$

Equations (4.14) allow one to compute λ_7, λ_8, λ_{10}, λ_{11}, λ_{22}, and λ_{25} by using as input the masses of the charged scalars and the masses and mixings of the neutral scalars. On the other hand, λ_4, λ_5, and λ_{19} constitute extra parameters that we input by hand — just as we did with λ_3 in section 3.

JHEP07(2021)195

UNI constraints. These constraints state that the moduli of the eigenvalues of some matrices must be smaller than 8π. The method for the derivation of those matrices in a general nHDM was explained in ref. [14]. In our specific case, the UNI constraints are (using $\Lambda_i \equiv |\lambda_i|$ for $i = 10, 11, 19, 22, 25$),

$$|\lambda_4 + \lambda_5 - \lambda_7 - \lambda_8| + \sqrt{(\lambda_4 - \lambda_5 - \lambda_7 + \lambda_8)^2 + 4\,|\lambda_{19} - \lambda_{22}|^2} < 16\pi, \tag{4.15a}$$

$$|\lambda_4 + \lambda_5 + \lambda_7 + \lambda_8| + \sqrt{(\lambda_4 - \lambda_5 + \lambda_7 - \lambda_8)^2 + 4\,|\lambda_{19} + \lambda_{22}|^2} < 16\pi, \tag{4.15b}$$

$$\lambda_1 + \sqrt{\lambda_1^2 + 4\,(\Lambda_{10}^2 + \Lambda_{11}^2 + 2\Lambda_{25}^2)} < 16\pi, \tag{4.15c}$$

$$\lambda_1 + \sqrt{\lambda_1^2 + 4\,(\lambda_7^2 + \lambda_8^2 + 2\Lambda_{22}^2)} < 16\pi, \tag{4.15d}$$

$$3\lambda_1 + \sqrt{9\lambda_1^2 + 4\left[(2\lambda_4 + \lambda_7)^2 + (2\lambda_5 + \lambda_8)^2 + 2\,|2\lambda_{19} + \lambda_{22}|^2\right]} < 16\pi, \tag{4.15e}$$

and the moduli of the eigenvalues of

$$\begin{pmatrix} \lambda_4 & \lambda_{10} & \lambda_{19}^* & \lambda_{25} \\ \lambda_{10}^* & \lambda_4 & \lambda_{25}^* & \lambda_{19} \\ \lambda_{19} & \lambda_{25} & \lambda_5 & \lambda_{11} \\ \lambda_{25}^* & \lambda_{19}^* & \lambda_{11}^* & \lambda_5 \end{pmatrix} \quad \text{and} \quad \begin{pmatrix} \lambda_4 + 2\lambda_7 & 3\lambda_{10} & \lambda_{19}^* + 2\lambda_{22}^* & 3\lambda_{25} \\ 3\lambda_{10}^* & \lambda_4 + 2\lambda_7 & 3\lambda_{25}^* & \lambda_{19} + 2\lambda_{22} \\ \lambda_{19} + 2\lambda_{22} & 3\lambda_{25} & \lambda_5 + 2\lambda_8 & 3\lambda_{11} \\ 3\lambda_{25}^* & \lambda_{19}^* + 2\lambda_{22}^* & 3\lambda_{11}^* & \lambda_5 + 2\lambda_8 \end{pmatrix} \tag{4.16}$$

must be smaller than 8π. In the inequalities (4.15), all the square roots are taken positive and $\lambda_1 = m_2^2/v^2$ is positive too.

Necessary conditions for boundedness-from-below (BFB). The quartic part of the potential, call it V_4, must be positive for all possible configurations of the scalar doublets, else the potential will be unbounded from below. In the configuration $\Phi_3 = 0$, the 3HDM becomes a 2HDM and one may use the BFB conditions for the 2HDM [18]:

$$\lambda_4 > 0, \quad \lambda_4 + \lambda_7 - \Lambda_{10} > 0. \tag{4.17}$$

Similarly, from the configuration $\Phi_2 = 0$,

$$\lambda_5 > 0, \quad \lambda_5 + \lambda_8 - \Lambda_{11} > 0. \tag{4.18}$$

We also consider the configuration

$$\Phi_1 = \begin{pmatrix} \varphi_1 \\ 0 \end{pmatrix}, \quad \Phi_2 = \begin{pmatrix} 0 \\ \varphi_2 \end{pmatrix}, \quad \Phi_3 = \begin{pmatrix} 0 \\ \varphi_3 \end{pmatrix}, \tag{4.19}$$

wherein $\Phi_1^\dagger \Phi_2 = \Phi_1^\dagger \Phi_3 = 0$ but $\Phi_2^\dagger \Phi_3 \neq 0$. Then,

$$V_4 \geq \frac{\lambda_1}{2}\, r_1^2 + r_1\left(\lambda_4 r_2 + \lambda_5 r_3 - 2\Lambda_{19}\sqrt{r_2 r_3}\right), \tag{4.20}$$

where $r_q := \Phi_q^\dagger \Phi_q$ for $q = 1, 2, 3$. By forcing $\lambda_4 r_2 + \lambda_5 r_3 - 2\Lambda_{19}\sqrt{r_2 r_3}$ to be positive for every positive r_2 and r_3, one obtains the necessary BFB condition

$$\lambda_4 + \lambda_5 - \sqrt{(\lambda_4 - \lambda_5)^2 + 4\,\Lambda_{19}^2} > 0. \tag{4.21}$$

JHEP07(2021)195

Sufficient BFB conditions. We know that $\Phi_q^\dagger\Phi_q\,\Phi_{q'}^\dagger\Phi_{q'} - \Phi_q^\dagger\Phi_{q'}\,\Phi_{q'}^\dagger\Phi_q \geq 0$ when $q \neq q'$. Therefore, we may parameterize

$$\Phi_1^\dagger\Phi_2 = \sqrt{r_1 r_2}\,k_{12}e^{i\phi_{12}}, \quad \Phi_1^\dagger\Phi_3 = \sqrt{r_1 r_3}\,k_{13}e^{i\phi_{13}}, \quad \Phi_2^\dagger\Phi_3 = \sqrt{r_2 r_3}\,k_{23}e^{i\phi_{23}}, \tag{4.22}$$

where k_{12}, k_{13}, and k_{23} are real numbers in the interval $[0,\,1]$. Then,

$$\begin{aligned}
V_4 = {} & \frac{\lambda_1}{2}\,r_1^2 + \lambda_4 r_1 r_2 + \lambda_5 r_1 r_3 + \lambda_7 r_1 r_2 k_{12}^2 + \lambda_8 r_1 r_3 k_{13}^2 + \Bigg\{ \frac{\lambda_{10}}{2}\,r_1 r_2 k_{12}^2 e^{2i\phi_{12}} \\
& + \frac{\lambda_{11}}{2}\,r_1 r_3 k_{13}^2 e^{2i\phi_{13}} + r_1\sqrt{r_2 r_3}\,\Big[\lambda_{19} k_{23} e^{i\phi_{23}} + \lambda_{22} k_{12} k_{13} e^{i(\phi_{13}-\phi_{12})} \\
& + \lambda_{25} k_{12} k_{13} e^{i(\phi_{13}+\phi_{12})}\Big] + \text{c.c.}\Bigg\} && \text{(4.23a)} \\
\geq {} & \frac{\lambda_1}{2}\,r_1^2 + \lambda_4 r_1 r_2 + \lambda_5 r_1 r_3 + (\lambda_7 - \Lambda_{10})\,r_1 r_2 k_{12}^2 + (\lambda_8 - \Lambda_{11})\,r_1 r_3 k_{13}^2 && \text{(4.23b)} \\
& - 2 r_1\sqrt{r_2 r_3}\,(\Lambda_{19} k_{23} + \Lambda k_{12} k_{13}) && \text{(4.23c)} \\
\geq {} & \frac{\lambda_1}{2}\,r_1^2 + \lambda_4 r_1 r_2 + \lambda_5 r_1 r_3 + (\lambda_7 - \Lambda_{10})\,r_1 r_2 k_{12}^2 + (\lambda_8 - \Lambda_{11})\,r_1 r_3 k_{13}^2 && \text{(4.23d)} \\
& - r_1\,(r_2 + r_3)\,(\Lambda_{19} k_{23} + \Lambda k_{12} k_{13}) && \text{(4.23e)} \\
\geq {} & \frac{\lambda_1}{2}\,r_1^2 + r_1 r_2\,\Big[\lambda_4 - \Lambda_{19} + (\lambda_7 - \Lambda_{10})\,k_{12}^2 - \Lambda\,k_{12} k_{13}\Big] && \text{(4.23f)} \\
& + r_1 r_3\,\Big[\lambda_5 - \Lambda_{19} + (\lambda_8 - \Lambda_{11})\,k_{13}^2 - \Lambda\,k_{12} k_{13}\Big] && \text{(4.23g)} \\
\geq {} & \frac{\lambda_1}{2}\,r_1^2 + r_1 r_2\,\Big[\lambda_4 - \Lambda_{19} + (\lambda_7 - \Lambda_{10})\,k_{12}^2 - \Lambda\,k_{12}\Big] && \text{(4.23h)} \\
& + r_1 r_3\,\Big[\lambda_5 - \Lambda_{19} + (\lambda_8 - \Lambda_{11})\,k_{13}^2 - \Lambda\,k_{13}\Big]\,. && \text{(4.23i)}
\end{aligned}$$

where $\Lambda := \Lambda_{22} + \Lambda_{25}$. Thus, denoting L_7 and L_8 the minimum values of $(\lambda_7 - \Lambda_{10})\,k_{12}^2 - \Lambda\,k_{12}$ and $(\lambda_8 - \Lambda_{11})\,k_{13}^2 - \Lambda\,k_{13}$, respectively, one has the sufficient BFB conditions [29]

$$\lambda_4 - \Lambda_{19} + L_7 > 0 \quad \text{and} \quad \lambda_5 - \Lambda_{19} + L_8 > 0. \tag{4.24}$$

It is easy to find that

$$L_7 = \begin{cases} \lambda_7 - \Lambda_{10} - \Lambda & \Leftarrow \lambda_7 - \Lambda_{10} < \dfrac{\Lambda}{2}, \\ -\dfrac{\Lambda^2}{4\,(\lambda_7 - \Lambda_{10})} & \Leftarrow \lambda_7 - \Lambda_{10} > \dfrac{\Lambda}{2}; \end{cases} \tag{4.25a}$$

$$L_8 = \begin{cases} \lambda_8 - \Lambda_{11} - \Lambda & \Leftarrow \lambda_8 - \Lambda_{11} < \dfrac{\Lambda}{2}, \\ -\dfrac{\Lambda^2}{4\,(\lambda_8 - \Lambda_{11})} & \Leftarrow \lambda_8 - \Lambda_{11} > \dfrac{\Lambda}{2}. \end{cases} \tag{4.25b}$$

5 Numerical results

In this section we display various scatter plots obtained by using the formulas in sections 3 and 4. In all the plots, we have restricted the Yukawa couplings e_2, e_3, f_2, and f_3 to have moduli smaller than 4π. The charged-scalar masses m_{C2} and m_{C3} were assumed to

JHEP07(2021)195

be between 150 GeV and 2 TeV. The neutral-scalar masses $m_3, \ldots, m_6$ were supposed to be lower than 2 TeV, but they have sometimes been allowed to be as low as 50 GeV. In practice, the upper bound on the scalar masses is mostly irrelevant, since the contributions of the new scalars to δg_L and δg_R tend to zero when the scalars become very heavy.

Constraints on the masses of the new scalars of the 2HDM and 3HDM may be derived from collider experiments on the production and subsequent decay of on-shell Higgs bosons. The sensitivity is limited by the kinematic reach of the experiments; moreover, the constraints usually depend on the assumed Yukawa couplings of the scalars and the fermions, which we do not want to specify in our work.

Constraints from the process $b \to s\gamma$ are most stringent. For a 2HDM of type II, a lower bound $m_{C2} > 480\,\text{GeV}$ at 95% CL has been derived in ref. [32]. However, in the case of the 3HDM, it has been shown in refs. [10, 33] that, due to the increased number of parameters, m_{C2} and m_{C3} may actually be lighter than the mass of top quark while complying with the constraints from $b \to s\gamma$.

In the 2HDM, a bound $m_{C2} \gtrsim 150\,\text{GeV}$ on the mass of the charged Higgs boson has been derived from searches at the LHC [34, 35]. Recent global fits [36, 37] give bounds on the scalar masses for various types of Yukawa couplings in the 2HDM. In ref. [36] it is claimed that the mass of the heavy CP-even Higgs boson $m_H > \{450, 700\}$ GeV, the mass of the CP-odd Higgs boson $m_A > \{500, 750\}\,\text{GeV}$, and the mass of the charged Higgs boson $m_{C2} > \{460, 740\}\,\text{GeV}$; the first values in the curled brackets correspond to the "lepton specific" type of 2HDM while the second values correspond to the type II and the "flipped" 2HDM. In the fit [37] of the aligned 2HDM one finds a lower bound of the new-scalar masses m_{C2}, m_3, and m_4 around 500 GeV or around 750 GeV, depending on the fitted mass range.

We depict in figure 6 the confrontation between experiment and the values of δg_L and δg_R attainable in the aligned 2HDM. One sees that, if one forces the 2HDM to comply with the S and T-oblique parameter constraints (3.16), then the 2HDM cannot achieve a better agreement with solution 1 for g_L and g_R than the SM; in particular, when one uses the A_b value (1.11), the 2HDM cannot even reach the 2σ interval. Only when one allows both for a laxer S- and T-oblique parameters constraints and for a very low neutral-scalar mass $m_3 \lesssim 60\,\text{GeV}$ are the central values of both solutions 1^{fit} and 1^{average} attainable. In the right panel of figure 6 one sees that, if both new neutral scalars of the 2HDM have masses larger than 150 GeV, then the fit to solution 1 is never better than in the SM case, even if one does not take into account the S and T-parameter constraints.[8]

In figure 7 we display the same points as in figure 6, now distinguishing the neutral-scalar contribution to δg_L from the charged-scalar contribution to the same quantity. The same exercise is performed in figure 8 for the contributions to δg_R. In the left panels of figures 7 and 8 one can see that the agreement of some blue points with solution 1^{fit} is

[8] We want to emphasize that the constraint on the oblique parameter S does not modify most of our figures much (notable exceptions are the blue areas in the left panels of figures 6–9); usually (but not always!), the points that comply with all other constraints also comply with the S ones. The oblique parameter S does not affect as much models with new scalars as models with new fermions, like for instance the ones in ref. [30].

JHEP07(2021)195

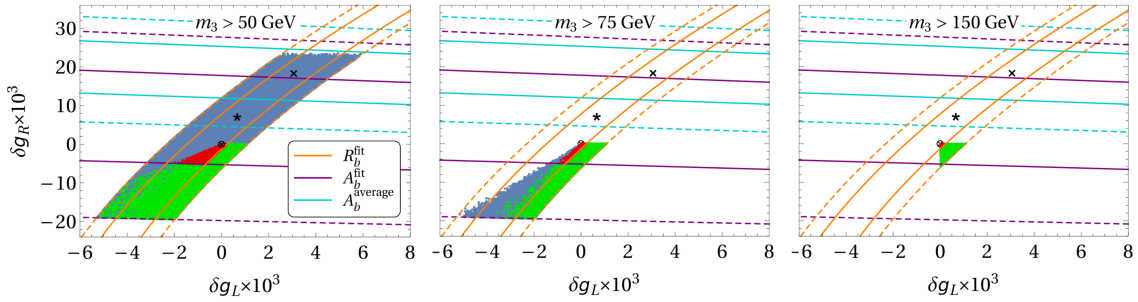

Figure 6. Scatter plot of values of δg_L and δg_R in the aligned 2HDM. A crossed circle marks the point $\delta g_L = \delta g_R = 0$. A star marks the best-fit point of solution $1^{\rm fit}$, and a cross the best-fit point of solution $1^{\rm average}$. The orange lines mark the 1σ (full lines) and 2σ (dashed lines) boundaries of the region determined by the experimental value (1.10a); similarly, the violet lines correspond to the value (1.10b) and the light-blue lines to the value (1.11). Red points agree with the 1σ intervals (1.10); green points agree with the 2σ, but not with the 1σ, intervals (1.10); and blue points agree either with the 1σ or the 2σ intervals (1.10). Both the red and the green points satisfy the 1σ limits in equation (3.16), while the blue points comply with laxer conditions where S can reach 2σ bounds and T can reach 3σ bounds in equation (3.16). Note that some blue points are underneath either red or green points. Left panel: both new neutral scalars have masses above 50 GeV; middle panel: both new neutral scalars have masses above 75 GeV; right panel: both new neutral scalars have masses above 150 GeV.

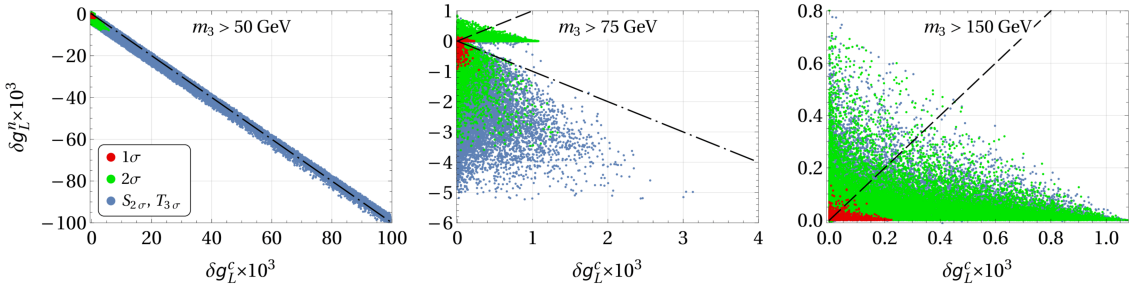

Figure 7. Scatter plot of δg_L^n *versus* δg_L^c in the aligned 2HDM. The displayed points and the colour code employed are the same as in figure 6. The dashed straight lines mark the condition $\delta g_L^n = \delta g_L^c$ and the dashed-dotted lines correspond to $\delta g_L^n = -\delta g_L^c$. Notice the vastly different scales in the three panels.

obtained not just by using very light neutral scalars and laxer oblique parameters S and T, but also through a fine-tuning where large neutral-scalar and charged-scalar contributions almost cancel each other. In the right panels of those figures one sees that, when both neutral scalars have masses above 150 GeV, the signs of the neutral-scalar and charged-scalar contributions are the same — this explains the agreement worse than in the SM observed in figure 6.

One also sees in figures 7 and 8 that the neutral-scalar contributions δg_L^n and δg_R^n are often comparable in size to, or even larger than, the charged-scalar contributions δg_L^c and δg_R^c, respectively. Thus, the usual practice of taking into account just the charged-scalar contribution may lead to erroneous results.

JHEP07(2021)195

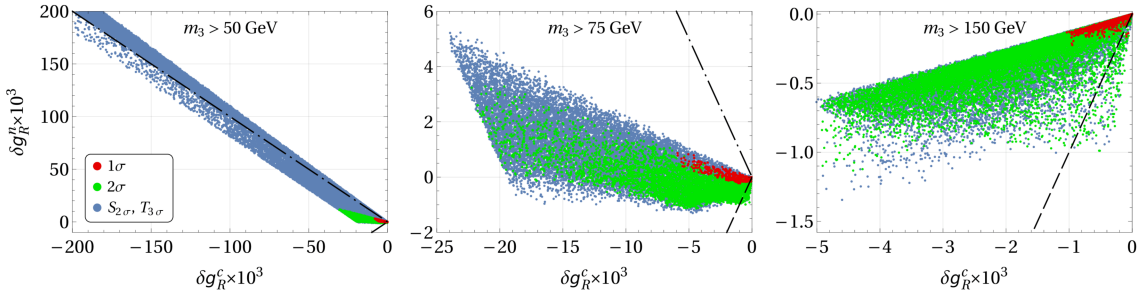

Figure 8. Scatter plot of δg_R^n *versus* δg_R^c in the aligned 2HDM. The displayed points and the colour code employed are the same as in figure 6. The dashed straight lines mark the condition $\delta g_R^n = \delta g_R^c$ and the dashed-dotted lines correspond to $\delta g_R^n = -\delta g_R^c$.

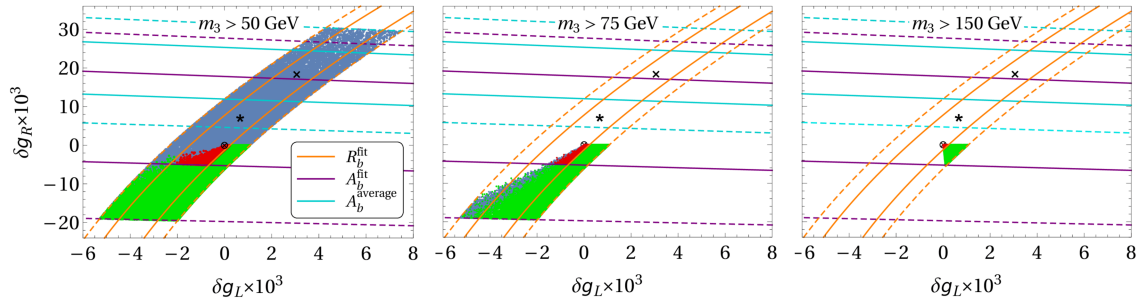

Figure 9. Scatter plot of values of δg_L and δg_R in the aligned 3HDM. All the conventions are the same as in figure 6.

One might hope the situation of disagreement with experiment to be milder in the 3HDM relative to the 2HDM, but one sees in figure 9 that this hardly happens. The agreement of the 3HDM with experiment may be better than the one of the 2HDM, but only in the case where very light neutral scalars exist. We have checked that, just as in the 2HDM, the better agreement occurs through an extensive finetuning where $\delta g_L^n \approx -\delta g_L^c$ and $\delta g_R^n \approx -\delta g_R^c$.

In figures 6–9 we have tried, and failed, to make the fits of solution 1 in the 2HDM and in the 3HDM better than in the SM. Things are different with solution 2, which the nHDM models can easily reproduce — with some caveats. We remind the reader that in solution 2 the parameter g_L is about the same as predicted by the SM, but the parameter g_R has sign opposite to the one in the SM, viz. $g_R \approx -0.08$ in solution 2 while $g_R \approx +0.08$ in the SM. In the left panel of figure 10 and in figure 11 we see how the fit of solution 2 works out in the case of the 2HDM. One sees that one can attain the 1σ intervals and the best-fit points both of solution 2^{fit} and of solution 2^{average}, but this requires (1) the new scalars of the 2HDM to be lighter than 440 GeV, (2) the Yukawa coupling f_2 to be quite large, and (3) the Yukawa coupling e_2 to be relatively small, possibly even zero. In practice, the upper bound on the masses of the scalars originates in the upper bound that unitarity imposes on f_2, as seen in the middle panel of figure 11; we have taken (rather arbitrarily) that upper bound to be $|f_2| < 4\pi \approx 12.5$. In the left panel of figure 11 one sees

JHEP07(2021)195

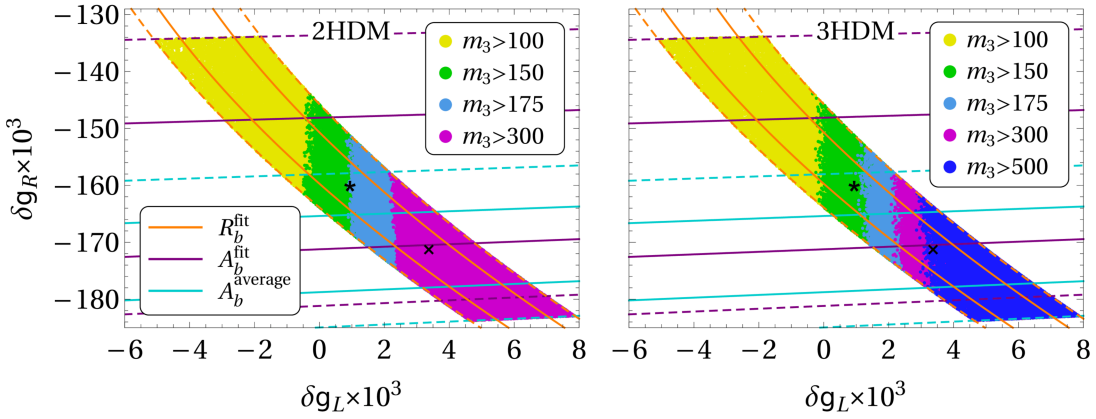

Figure 10. Scatter plot of values of δg_L and δg_R in the aligned 2HDM (left panel) and in the aligned 3HDM (right panel) that suit the solution 2 for R_b and A_b. All the points depicted comply with the S and T-oblique parameters constraint of equation (3.16). A star marks the best-fit point of solution 2^{fit}, and a cross the best-fit point of solution 2^{average}. The orange lines mark the 1σ (full lines) and 2σ (dashed lines) boundaries of the region determined by the experimental value (1.10a); similarly, the violet lines correspond to the value (1.10b) and the light-blue lines to the value (1.11). Blue points have new neutral scalars heavier than 500 GeV, pink points have them heavier than 300 GeV, light blue points have the lightest new neutral scalar in between 175 GeV and 300 GeV, green points have it in between 150 GeV and 175 GeV, and yellow points have it between 100 GeV and 150 GeV.

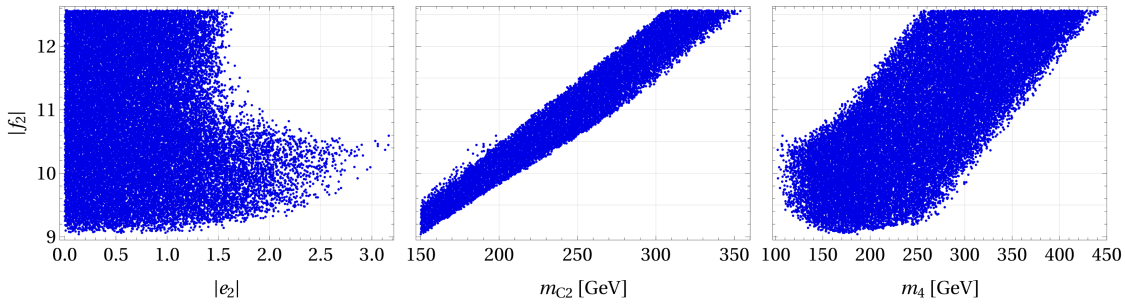

Figure 11. Scatter plot of 2HDM points that obey the S- and T-oblique parameters constraints, fit solution 2^{average} at the 1σ level, and have $m_3 > 100$ GeV.

that $|f_2|$ must be larger than 9 anyway. It is also clear from figure 10 that, the lighter the new scalars are allowed to be, the easier it is to reproduce solution 2; moreover, it is easier to reproduce solution 2^{average}, viz. with the value (1.11) for A_b, than solution 2^{fit}, viz. with the value (1.10b) for A_b, because solution 2^{average} does not necessitate m_3 to be as low as solution 2^{fit}.

In the right panel of figure 10 and in figures 12 and 13 we illustrate the fitting of solution 2 in the 3HDM. Comparing the left and right panels of figure 10, we see that the 2HDM and the 3HDM give similar results, but in the 3HDM it is possible to reach solution 2^{average} with larger masses of the new scalars. Indeed, in the 3HDM the lightest neutral scalar m_3 may be as heavy as 620 GeV, while in the 2HDM $m_3 < 420$ GeV. Like in

JHEP07(2021)195

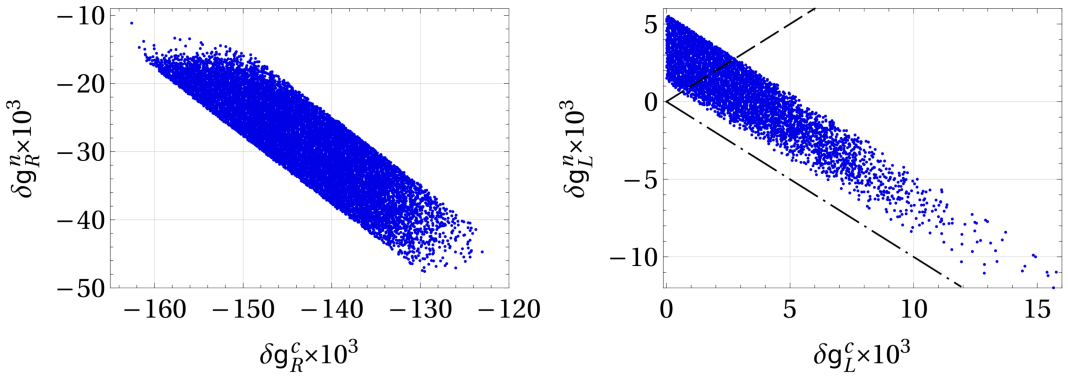

Figure 12. Scatter plot of 3HDM points that obey the S- and T-oblique parameters constraints, fit solution 2^{average} at the 1σ level, and have $m_3 > 100\,\text{GeV}$. Left panel: the neutral-scalar contribution to δg_R *versus* the charged-scalar contribution to the same quantity. Right panel: the same for δg_L instead of δg_R. In the right panel, the dashed line marks the condition $\delta g_L^n = \delta g_L^c$ and the dashed-dotted line corresponds to $\delta g_L^n = -\delta g_L^c$.

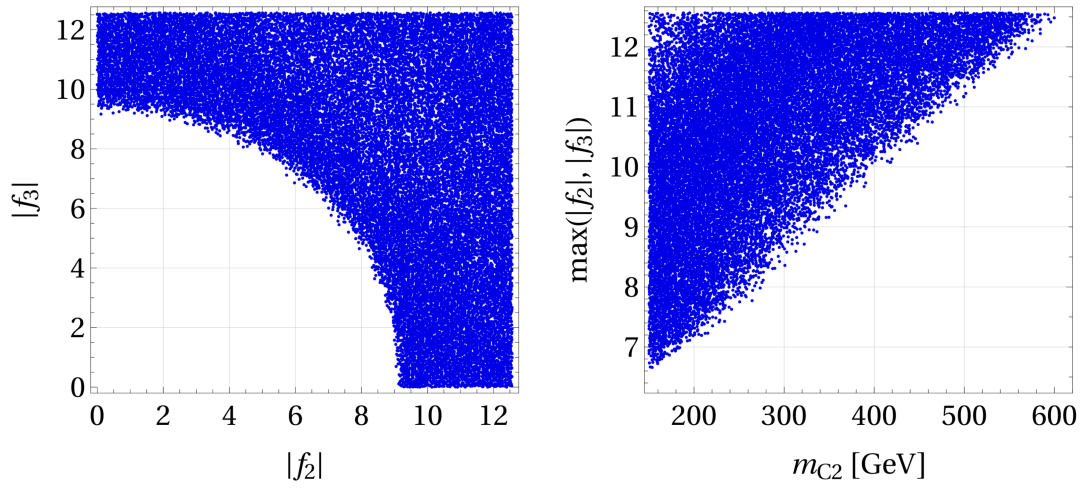

Figure 13. Scatter plot of 3HDM points that obey the S- and T-oblique parameters constraints, fit solution 2^{average} at the 1σ level, and have $m_3 > 100\,\text{GeV}$. Left panel: the modulus of the Yukawa coupling f_3 *versus* the modulus of f_2. Right panel: the largest of the two Yukawa couplings f_2 and f_3 *versus* the mass of the lightest charged scalar.

figure 11, in figures 12 and 13 we have used points that satisfy the S- and T-parameters 1σ bounds (3.16), that fall into the 1σ intervals of δg_L and δg_R for solution 2^{average},[9] and that have $m_3 > 100\,\text{GeV}$. In figure 12 we display the charged- and neutral-scalar contributions to δg_L and δg_R. One sees that solution 2 may be considered a finetuning, with $|\delta g_R^c| \gg |\delta g_R^n, \delta g_L^c, \delta g_L^n|$. We stress once again that the neutral-scalar contributions are as instrumental as the charged-scalar ones in obtaining decent fits. In figure 13 we illustrate the moduli of the f Yukawa couplings and their relationship to the masses of the

[9]The fit of solution 2^{fit} is not qualitatively different from the one of 2^{average}; we concentrate on the latter just for the sake of simplicity.

JHEP07(2021)195

scalars. One sees in the left panel that there is a bound $\sqrt{|f_2|^2 + |f_3|^2} \gtrsim 9$, but each one of the Yukawa couplings f_2 and f_3 may separately vanish. In the right panel one observes that there is a simple straight-line correlation between the maximum possible value for the mass of the lightest charged scalar, m_{C2}, and the minimum possible value for the largest of the Yukawa couplings f_2 and f_3. It is worth pointing out that in the 3HDM, just as in the 2HDM, the masses m_3, m_4, and m_{C2} must be low (because of the unitarity upper bound on the f Yukawa couplings), but in the 3HDM the masses m_5, m_6, and m_{C3} do not need to be low — they may be of order TeV.

6 Conclusions

The Standard Model (SM) has a slight problem in fitting the $Zb\bar{b}$ vertex, since it produces a g_R smaller than what is needed to reproduce the fit (1.10); this discrepancy becomes larger when one uses for A_b the value (1.11). In this paper we have found that this small problem can only worsen when one extends the SM through a nHDM. This is because the contributions of the new scalars usually produce a negative δg_R, i.e. they go in the wrong direction to alleviate the problem, aggravating it instead.

There is one possible escape from this conclusion if the extra neutral scalars of the nHDM are very light, i.e. lighter than the Fermi scale, because the contribution of the neutral scalars to δg_R may in that case be positive and partially compensate for the inevitably negative contribution of the charged scalars. This is a contrived effort, though, both because it is experimentally difficult to accomodate very light neutral scalars and because, from the theoretical side, light neutral scalars together with heavy charged scalars easily lead to a much-too-large oblique parameter T.

In this paper we have considered the possibility that, in nHDM models, we might look instead at an alternative fit of the $Zb\bar{b}$ vertex, wherein g_R has the opposite sign from the one predicted by the SM. This is what we have called "solution 2" in table 1. That solution necessitates a very large negative δg_R (together with a small δg_L), that may seem like a finetuning, but is easy to obtain in a nHDM. This solution, though, also works only if the new scalars are relatively light and if at least one of the Yukawa couplings denoted f_k in equation (2.5) is quite large, viz. larger than 9 or so.

Acknowledgments

D.J. thanks the Lithuanian Academy of Sciences for financial support through projects DaFi2019 and DaFi2021. L.L. thanks the Portuguese Foundation for Science and Technology for support through CERN/FIS-PAR/0004/2019, CERN/FIS-PAR/0008/2019, PTDC/FIS-PAR/29436/2017, UIDB/00777/2020, and UIDP/00777/2020.

A Definition and measurements of R_b and A_b

The experimental quantities R_b and A_b are defined for e^+e^- collisions at the Z^0 peak, i.e. with $\sqrt{s} \approx m_Z$. Let the quark q ($q = u, d, s, c, b$) couple to the Z^0 as

$$\mathcal{L}_{Zqq} = \frac{g}{c_w} Z_\mu \, \bar{q} \gamma^\mu \left(g_{Lq} P_L + g_{Rq} P_R \right) q. \tag{A.1}$$

JHEP07(2021)195

One has

$$g_{Lq} = \frac{1}{2} - \frac{2s_w^2}{3}, \qquad g_{Rq} = -\frac{2s_w^2}{3} \tag{A.2}$$

for $q = c$ and $q = u$, and

$$g_{Lq} = \frac{s_w^2}{3} - \frac{1}{2}, \qquad g_{Rq} = \frac{s_w^2}{3} \tag{A.3}$$

for $q = b$, $q = s$, and $q = d$. The probability that one produces a $q\bar{q}$ pair in an e^+e^- collision at the Z^0 peak is, in the absence of QCD, QED, and mass corrections proportional to

$$s_q = 2\left(g_{Lq}^2 + g_{Rq}^2\right). \tag{A.4}$$

One finds from equations (A.2)–(A.4) that

$$s_c + s_u + s_s + s_d = 2 - 4s_w^2 + \frac{40}{9}\, s_w^4 \approx 1.32827. \tag{A.5}$$

The experimental definition of R_b is

$$R_b = \frac{\Gamma_{b\bar{b}}}{\Gamma_{\text{hadrons}}} \tag{A.6}$$

in e^+e^- collisions at the Z^0 peak; thus, R_b is the fraction of the produced hadrons that contain a $b\bar{b}$ pair. Clearly, in the absence of QCD, QED, and mass corrections,

$$R_b = \frac{s_b}{s_b + s_c + s_u + s_s + s_d} \tag{A.7a}$$

$$= \frac{9 - 12s_w^2 + 8s_w^4}{45 - 84s_w^2 + 88s_w^4} \approx 0.21937. \tag{A.7b}$$

When one includes QCD, QED, and mass corrections equation (A.7a) gets substituted by equation (1.7) and R_b decreases from the value in equation (A.7b) to the SM prediction [4] 0.21581. Similarly, $s_c + s_u + s_s + s_d$ becomes 1.3184 instead of 1.32827 as in equation (A.5).

If the mass of the bottom quark was zero, equation (1.5) would read

$$A_b = \frac{g_L^2 - g_R^2}{g_L^2 + g_R^2} = \frac{9 - 12s_w^2}{9 - 12s_w^2 + 8s_w^4} \approx 0.94059 \tag{A.8}$$

at the tree level. The quantity A_b was accessed at LEP 1 through the forward-backward asymmetry of the produced $b\bar{b}$ quark pairs,

$$A_{\text{FB}}^{0,b} = \frac{3}{4}\, A_e A_b, \tag{A.9}$$

where A_e, that is

$$A_e = \frac{1 - 4s_w^2}{1 - 4s_w^2 + 8s_w^4} \approx 0.21065 \tag{A.10}$$

at the tree level, can be extracted from other experiments. Equation (A.9) is the limit of

$$A_{\text{FB}}^{P_e,b} = \frac{3}{4}\, \frac{A_e + P_e}{1 + A_e P_e}\, A_b \tag{A.11}$$

JHEP07(2021)195

when the polarization P_e of the electron beam is zero. The SLD Collaboration has used polarized beams ($P_e = 1$) and therefore it could directly access

$$\frac{3}{4} A_b = \frac{\sigma_{LF} + \sigma_{RB} - \sigma_{LB} - \sigma_{RF}}{\sigma_{LF} + \sigma_{RB} + \sigma_{LB} + \sigma_{RF}}, \tag{A.12}$$

where the subscripts L and R refer to the electron's polarization and the subscripts F and B refer to the forward or backward direction of travel of the final-state bottom quarks.

The value of A_b obtained from the SLD measurement is $A_b^{\text{fit}} = 0.923 \pm 0.020$ and is 0.6σ below the SM value [1]. However, this good agreement only applies to the overall fit of many observables. Extracting A_b from $A_{\text{FB}}^{0,b}$ when $A_e = 0.1501 \pm 0.0016$ leads to $A_b = 0.885 \pm 0.0017$, which is 2.9σ below the SM prediction. The combined value $A_b = 0.901 \pm 0.013$ deviates from the SM value by 2.6σ. These discrepancies in A_b could be an evidence of New Physics, but they could also be due to a statistical fluctuation or another experimental effect in one of asymmetries; more precise experiments are needed.

A direct measurement of the $Zb\bar{b}$ couplings at the LHC is challenging because of the large backgrounds in the detection of a Z^0 decaying into a bottom quark-antiquark pair. A recent study [6] has proposed a novel method to probe the anomalous $Zb\bar{b}$ couplings through the measurement of the cross section of the associated production $gg \to Zh$ at the High Luminosity LHC.

Lepton colliders of the next generation, vg. the CEPC, ILC, or FCC-ee offer great opportunities for further studies of the $Zb\bar{b}$ vertex, because they could collect a large amount of data around the Z^0 pole. In the analysis [31] there is a list of the observables that are most important for improving the constraints on the $Zb\bar{b}$ coupling, and of the expected precision reach of those three proposed future e^+e^- colliders. These estimates, for the observables directly related to the $Zb\bar{b}$ coupling, are summarized in table 2. We see that, with an increase of precision of more than one order of magnitude, a future collider has the potential to solve the $A_{\text{FB}}^{0,b}$ discrepancy found at LEP. If its results are SM-like, a future lepton collider can provide strong constraints on models beyond the SM; if the $A_{\text{FB}}^{0,b}$ discrepancy found at LEP does come from New Physics, then any of the three next-generation e^+e^- colliders will be able to rule out the SM with more than 5σ significance [31].

B General formula for the neutral-scalar contribution

According to ref. [15], the contributions to δg_L and δg_R of loops with internal lines of neutral scalars and bottom quarks are the sums of three types of Feynman diagrams. Thus,

$$\delta g_L^n = \delta g_L^n(a) + \delta g_L^n(b) + \delta g_L^n(c), \quad \delta g_R^n = \delta g_R^n(a) + \delta g_R^n(b) + \delta g_R^n(c). \tag{B.1}$$

Equations (24), (42), and (46) of ref. [15] inform us that

$$\delta g_L^n(a) = \frac{-i}{32\pi^2} \sum_{l,l'=1}^{2n} \mathcal{A}_{ll'} \left(\mathcal{V}^T F\right)_l \left(\mathcal{V}^\dagger F^*\right)_{l'} C_{00}\left(0, m_Z^2, 0, 0, m_{l'}^2, m_l^2\right), \tag{B.2a}$$

$$\delta g_R^n(a) = \frac{-i}{32\pi^2} \sum_{l,l'=1}^{2n} \mathcal{A}_{ll'} \left(\mathcal{V}^\dagger F^*\right)_l \left(\mathcal{V}^T F\right)_{l'} C_{00}\left(0, m_Z^2, 0, 0, m_{l'}^2, m_l^2\right), \tag{B.2b}$$

JHEP07(2021)195

Observable	Current measurement	Precision			
		Current	CEPC	ILC	FCC-ee
R_b	0.21629	0.00066 (0.00050)	0.00017 (0.00016)	0.00014	0.00006 (0.00006)
$A_{\rm FB}^{0,b}$	0.0996	0.0016 (0.0007)	0.00015 (0.00014)		
A_b	0.923	0.020		0.001	0.00021 (0.00015)
# of Z^0s	$\sim 2\times 10^7$		$\sim 2\times 10^9$	$\sim 10^9$	$\sim 10^{12}$

Table 2. The estimated precision reach for $Zb\bar{b}$ observables at future e^+e^- colliders according to ref. [31]. The present result for each observable is shown in the second column. The third column shows the σ of the present measurements at LEP and SLC, respectively, while the other columns show the estimates of the precision reach for the future colliders. In each entry, the number in the top line shows the total uncertainty and the number (in parenthesis) in the bottom line shows the systematic uncertainty. The last row shows the expected number of Z^0 events that will be collected.

where $\mathcal{A}$ is the matrix defined in equation (2.4), and

$$F = \begin{pmatrix} \sqrt{2}m_b/v \\ f_2 \\ \vdots \\ f_n \end{pmatrix} \tag{B.3}$$

is a vector formed by Yukawa coupling constants. Now,

$$C_{00}\left(0,\, m_Z^2,\, 0,\, 0,\, m_{l'}^2,\, m_l^2\right) = C_{00}\left(0,\, m_Z^2,\, 0,\, 0,\, m_l^2,\, m_{l'}^2\right), \tag{B.4}$$

while $\mathcal{A}_{ll'} = -\mathcal{A}_{l'l}$. Therefore, equations (B.2) may be rewritten

$$\delta g_L^n(a) = \frac{1}{16\pi^2}\sum_{l=2}^{2n-1}\sum_{l'=l+1}^{2n}\mathcal{A}_{ll'}\,\mathrm{Im}\left[\left(\mathcal{V}^T F\right)_l\left(\mathcal{V}^\dagger F^*\right)_{l'}\right] C_{00}\left(0,\, m_Z^2,\, 0,\, 0,\, m_{l'}^2,\, m_l^2\right), \tag{B.5a}$$

$$\delta g_R^n(a) = -\delta g_L^n(a), \tag{B.5b}$$

where we have dropped from the sum over the scalars the Standard-Model contribution proportional to $\mathcal{A}_{12}$.

According to equations (2), (25), and (26) of ref. [15],

$$\delta g_L^n(b) + \delta g_L^n(c) = \frac{1}{16\pi^2}\sum_{l=2}^{2n}\left|\left(\mathcal{V}^T F\right)_l\right|^2\theta\left(m_l^2\right), \tag{B.6a}$$

$$\delta g_R^n(b) + \delta g_R^n(c) = \frac{1}{16\pi^2}\sum_{l=2}^{2n}\left|\left(\mathcal{V}^T F\right)_l\right|^2\lambda\left(m_l^2\right), \tag{B.6b}$$

JHEP07(2021)195

where

$$\theta\left(m_l^2\right) := \frac{s_w^2}{6}\left[2\,C_{00}\left(0,\, m_Z^2,\, 0,\, m_l^2,\, 0,\, 0\right) - \frac{1}{2}\right.$$
$$\left. - m_Z^2\, C_{12}\left(0,\, m_Z^2,\, 0,\, m_l^2,\, 0,\, 0\right)\right] + \left(\frac{s_w^2}{6} - \frac{1}{4}\right) B_1\left(0,\, 0,\, m_l^2\right), \tag{B.7a}$$

$$\lambda\left(m_l^2\right) := \left(\frac{s_w^2}{6} - \frac{1}{4}\right)\left[2\,C_{00}\left(0,\, m_Z^2,\, 0,\, m_l^2,\, 0,\, 0\right) - \frac{1}{2}\right.$$
$$\left. - m_Z^2\, C_{12}\left(0,\, m_Z^2,\, 0,\, m_l^2,\, 0,\, 0\right)\right] + \frac{s_w^2}{6} B_1\left(0,\, 0,\, m_l^2\right). \tag{B.7b}$$

We now write

$$\mathcal{V} = \mathcal{R} + i\mathcal{I}, \tag{B.8}$$

where the $n \times 2n$ matrices $\mathcal{R}$ and $\mathcal{I}$ are real and satisfy

$$\mathcal{R}\mathcal{R}^T = \mathcal{I}\mathcal{I}^T = \mathbb{1}_{n_d \times n_d}, \quad \mathcal{R}\mathcal{I}^T = \mathcal{I}\mathcal{R}^T = 0_{n_d \times n_d}, \tag{B.9}$$

cf. equation (2.3). From equation (B.8),

$$\mathcal{A} := \mathrm{Im}\left(\mathcal{V}^\dagger \mathcal{V}\right) = \mathcal{R}^T\mathcal{I} - \mathcal{I}^T\mathcal{R}. \tag{B.10}$$

It follows that

$$\sum_{l'=1}^{2n} \mathcal{A}_{ll'}\left(\mathcal{V}^\dagger F^*\right)_{l'} = -i\left(\mathcal{V}^\dagger F^*\right)_l, \quad \sum_{l=1}^{2n}\left(\mathcal{V}^T F\right)_l \mathcal{A}_{ll'} = -i\left(\mathcal{V}^T F\right)_{l'}. \tag{B.11}$$

Therefore, from equations (B.6),

$$\delta g_L^n(b) + \delta g_L^n(c) = \frac{1}{32\pi^2}\left[\sum_{l=2}^{2n}\left(\mathcal{V}^T F\right)_l\left(\mathcal{V}^\dagger F^*\right)_l \theta\left(m_l^2\right)\right.$$
$$\left. + \sum_{l'=2}^{2n}\left(\mathcal{V}^T F\right)_{l'}\left(\mathcal{V}^\dagger F^*\right)_{l'}\theta\left(m_{l'}^2\right)\right] \tag{B.12a}$$

$$= \frac{1}{32\pi^2}\left\{\sum_{l=2}^{2n}\left(\mathcal{V}^T F\right)_l\left[i\sum_{l'=1}^{2n}\mathcal{A}_{ll'}\left(\mathcal{V}^\dagger F^*\right)_{l'}\right]\theta\left(m_l^2\right)\right.$$
$$\left. + \sum_{l'=2}^{2n}\left[i\sum_{l=1}^{2n}\left(\mathcal{V}^T F\right)_l \mathcal{A}_{ll'}\right]\left(\mathcal{V}^\dagger F^*\right)_{l'}\theta\left(m_{l'}^2\right)\right\} \tag{B.12b}$$

$$= \frac{i}{32\pi^2}\sum_{l,l'=1}^{2n}\left(\mathcal{V}^T F\right)_l \mathcal{A}_{ll'}\left(\mathcal{V}^\dagger F^*\right)_{l'}\left[\theta\left(m_l^2\right) + \theta\left(m_{l'}^2\right)\right], \tag{B.12c}$$

$$\delta g_R^n(b) + \delta g_R^n(c) = \frac{i}{32\pi^2}\sum_{l,l'=1}^{2n}\left(\mathcal{V}^T F\right)_l \mathcal{A}_{ll'}\left(\mathcal{V}^\dagger F^*\right)_{l'}\left[\lambda\left(m_l^2\right) + \lambda\left(m_{l'}^2\right)\right]. \tag{B.12d}$$

JHEP07(2021)195

Thus, from equations (B.1) and (B.2),

$$\delta g_L^n = \frac{-i}{32\pi^2} \sum_{l,l'=1}^{2n} \mathcal{A}_{ll'} \left(\mathcal{V}^T F\right)_l \left(\mathcal{V}^\dagger F^*\right)_{l'} \left[C_{00}\left(0,\, m_Z^2,\, 0,\, 0,\, m_{l'}^2,\, m_l^2\right)\right.$$
$$\left. -\theta\left(m_l^2\right) - \theta\left(m_{l'}^2\right)\right], \tag{B.13a}$$

$$\delta g_R^n = \frac{-i}{32\pi^2} \sum_{l,l'=1}^{2n} \mathcal{A}_{ll'} \left(\mathcal{V}^T F\right)_l \left(\mathcal{V}^\dagger F^*\right)_{l'} \left[-C_{00}\left(0,\, m_Z^2,\, 0,\, 0,\, m_{l'}^2,\, m_l^2\right)\right.$$
$$\left. -\lambda\left(m_l^2\right) - \lambda\left(m_{l'}^2\right)\right]. \tag{B.13b}$$

We define the functions

$$h_L\left(m_{l'}^2,\, m_l^2\right) := -C_{00}\left(0,\, m_Z^2,\, 0,\, 0,\, m_{l'}^2,\, m_l^2\right) + \theta\left(m_{l'}^2\right) + \theta\left(m_l^2\right), \tag{B.14a}$$

$$h_R\left(m_{l'}^2,\, m_l^2\right) := C_{00}\left(0,\, m_Z^2,\, 0,\, 0,\, m_{l'}^2,\, m_l^2\right) + \lambda\left(m_{l'}^2\right) + \lambda\left(m_l^2\right). \tag{B.14b}$$

These functions are symmetric under the interchange of their two arguments:

$$h_L\left(m_{l'}^2,\, m_l^2\right) = h_L\left(m_l^2,\, m_{l'}^2\right), \quad h_R\left(m_{l'}^2,\, m_l^2\right) = h_R\left(m_l^2,\, m_{l'}^2\right). \tag{B.15}$$

Moreover, by utilizing equations (21) of ref. [15] it is easy to show that, although the functions $\theta\left(m_l^2\right)$, $\lambda\left(m_l^2\right)$, and $C_{00}\left(0,\, m_Z^2,\, 0,\, 0,\, m_{l'}^2,\, m_l^2\right)$ contain divergences, the functions $h_L\left(m_{l'}^2,\, m_l^2\right)$ and $h_R\left(m_{l'}^2,\, m_l^2\right)$ do not. From equation (B.13) we obtain

$$\delta g_L^n = \frac{1}{16\pi^2} \sum_{l=2}^{2n-1} \sum_{l'=l+1}^{2n} \mathcal{A}_{ll'}\, \mathrm{Im}\left[\left(\mathcal{V}^\dagger F^*\right)_l \left(\mathcal{V}^T F\right)_{l'}\right] h_L\left(m_{l'}^2,\, m_l^2\right), \tag{B.16a}$$

$$\delta g_R^n = \delta g_L^n \left[h_L\left(m_{l'}^2,\, m_l^2\right) \to h_R\left(m_{l'}^2,\, m_l^2\right)\right]. \tag{B.16b}$$

Thus, the functions h_L and h_R are crucial in the computation of the neutral-scalar contributions to δg_L and δg_R, respectively. Those functions were not explicitly defined in ref. [15], even though they were utilized in that paper.

Open Access. This article is distributed under the terms of the Creative Commons Attribution License (CC-BY 4.0), which permits any use, distribution and reproduction in any medium, provided the original author(s) and source are credited.

References

[1] Particle Data Group collaboration, *Review of Particle Physics*, *PTEP* **2020** (2020) 083C01 [INSPIRE].

[2] J.H. Field, *Indications for an anomalous right-handed coupling of the b quark from a model independent analysis of LEP and SLD data on Z decays*, *Mod. Phys. Lett. A* **13** (1998) 1937 [hep-ph/9801355] [INSPIRE].

[3] H.E. Haber and H.E. Logan, *Radiative corrections to the $Zb\bar{b}$ vertex and constraints on extended Higgs sectors*, *Phys. Rev. D* **62** (2000) 015011 [hep-ph/9909335] [INSPIRE].

JHEP07(2021)195

[4] J. Erler and A. Freitas, *Electroweak model and constraints on new physics*, in *Review of Particle Physics*, *PTEP* **2020** (2020) 083C01, pg. 180.

[5] D. Choudhury, T.M.P. Tait and C.E.M. Wagner, *Beautiful mirrors and precision electroweak data*, *Phys. Rev. D* **65** (2002) 053002 [hep-ph/0109097] [INSPIRE].

[6] B. Yan and C.P. Yuan, *The anomalous $Zb\bar{b}$ couplings: From LEP to LHC*, arXiv:2101.06261 [INSPIRE].

[7] G.C. Branco, P.M. Ferreira, L. Lavoura, M.N. Rebelo, M. Sher and J.P. Silva, *Theory and phenomenology of two-Higgs-doublet models*, *Phys. Rept.* **516** (2012) 1 [arXiv:1106.0034] [INSPIRE].

[8] A. Pich and P. Tuzon, *Yukawa Alignment in the Two-Higgs-Doublet Model*, *Phys. Rev. D* **80** (2009) 091702 [arXiv:0908.1554] [INSPIRE].

[9] A. Pilaftsis, *Symmetries for standard model alignment in multi-Higgs doublet models*, *Phys. Rev. D* **93** (2016) 075012 [arXiv:1602.02017] [INSPIRE].

[10] H.E. Logan, S. Moretti, D. Rojas-Ciofalo and M. Song, *CP violation from charged Higgs bosons in the three Higgs doublet model*, arXiv:2012.08846 [INSPIRE].

[11] V. Keus, S.F. King and S. Moretti, *Three-Higgs-doublet models: symmetries, potentials and Higgs boson masses*, *JHEP* **01** (2014) 052 [arXiv:1310.8253] [INSPIRE].

[12] I.P. Ivanov and E. Vdovin, *Classification of finite reparametrization symmetry groups in the three-Higgs-doublet model*, *Eur. Phys. J. C* **73** (2013) 2309 [arXiv:1210.6553] [INSPIRE].

[13] D. Das and I. Saha, *Alignment limit in three Higgs-doublet models*, *Phys. Rev. D* **100** (2019) 035021 [arXiv:1904.03970] [INSPIRE].

[14] M.P. Bento, H.E. Haber, J.C. Romão and J.P. Silva, *Multi-Higgs doublet models: physical parametrization, sum rules and unitarity bounds*, *JHEP* **11** (2017) 095 [arXiv:1708.09408] [INSPIRE].

[15] D. Fontes, L. Lavoura, J.C. Romão and J.P. Silva, *One-loop corrections to the $Zb\bar{b}$ vertex in models with scalar doublets and singlets*, *Nucl. Phys. B* **958** (2020) 115131 [arXiv:1910.11886] [INSPIRE].

[16] A. Denner, S. Dittmaier and L. Hofer, *Collier: a fortran-based Complex One-Loop LIbrary in Extended Regularizations*, *Comput. Phys. Commun.* **212** (2017) 220 [arXiv:1604.06792] [INSPIRE].

[17] H.H. Patel, *Package-X: A Mathematica package for the analytic calculation of one-loop integrals*, *Comput. Phys. Commun.* **197** (2015) 276 [arXiv:1503.01469] [INSPIRE].

[18] G.C. Branco, P.M. Ferreira, L. Lavoura, M.N. Rebelo, M. Sher and J.P. Silva, *Theory and phenomenology of two-Higgs-doublet models*, *Phys. Rept.* **516** (2012) 1 [arXiv:1106.0034] [INSPIRE].

[19] A. Barroso, P.M. Ferreira, I.P. Ivanov, R. Santos and J.P. Silva, *Evading death by vacuum*, *Eur. Phys. J. C* **73** (2013) 2537 [arXiv:1211.6119] [INSPIRE].

[20] I.P. Ivanov, *Minkowski space structure of the Higgs potential in 2HDM*, *Phys. Rev. D* **75** (2007) 035001 [*Erratum ibid.* **76** (2007) 039902] [hep-ph/0609018] [INSPIRE].

[21] I.P. Ivanov, *Minkowski space structure of the Higgs potential in 2HDM. II. Minima, symmetries, and topology*, *Phys. Rev. D* **77** (2008) 015017 [arXiv:0710.3490] [INSPIRE].

JHEP07(2021)195

[22] I.P. Ivanov and J.P. Silva, *Tree-level metastability bounds for the most general two Higgs doublet model*, *Phys. Rev. D* **92** (2015) 055017 [arXiv:1507.05100] [INSPIRE].

[23] M.E. Peskin and T. Takeuchi, *A New constraint on a strongly interacting Higgs sector*, *Phys. Rev. Lett.* **65** (1990) 964 [INSPIRE].

[24] G. Altarelli and R. Barbieri, *Vacuum polarization effects of new physics on electroweak processes*, *Phys. Lett. B* **253** (1991) 161 [INSPIRE].

[25] M.E. Peskin and T. Takeuchi, *Estimation of oblique electroweak corrections*, *Phys. Rev. D* **46** (1992) 381 [INSPIRE].

[26] G. Altarelli, R. Barbieri and S. Jadach, *Toward a model independent analysis of electroweak data*, *Nucl. Phys. B* **369** (1992) 3 [*Erratum ibid.* **376** (1992) 444] [INSPIRE].

[27] W. Grimus, L. Lavoura, O.M. Ogreid and P. Osland, *The Oblique parameters in multi-Higgs-doublet models*, *Nucl. Phys. B* **801** (2008) 81 [arXiv:0802.4353] [INSPIRE].

[28] W. Grimus, L. Lavoura, O.M. Ogreid and P. Osland, *A precision constraint on multi-Higgs-doublet models*, *J. Phys. G* **35** (2008) 075001 [arXiv:0711.4022] [INSPIRE].

[29] P.M. Ferreira, I.P. Ivanov, E. Jiménez, R. Pasechnik and H. Serôdio, *CP4 miracle: shaping Yukawa sector with CP symmetry of order four*, *JHEP* **01** (2018) 065 [arXiv:1711.02042] [INSPIRE].

[30] B. Batell, S. Gori and L.-T. Wang, *Higgs Couplings and Precision Electroweak Data*, *JHEP* **01** (2013) 139 [arXiv:1209.6382] [INSPIRE].

[31] S. Gori, J. Gu and L.-T. Wang, *The $Zb\bar{b}$ couplings at future e^+ e^- colliders*, *JHEP* **04** (2016) 062 [arXiv:1508.07010] [INSPIRE].

[32] M. Misiak et al., *Updated NNLO QCD predictions for the weak radiative B-meson decays*, *Phys. Rev. Lett.* **114** (2015) 221801 [arXiv:1503.01789] [INSPIRE].

[33] A.G. Akeroyd, S. Moretti, K. Yagyu and E. Yildirim, *Light charged Higgs boson scenario in 3-Higgs doublet models*, *Int. J. Mod. Phys. A* **32** (2017) 1750145 [arXiv:1605.05881] [INSPIRE].

[34] CMS collaboration, *Search for a charged Higgs boson in pp collisions at $\sqrt{s} = 8$ TeV*, *JHEP* **11** (2015) 018 [arXiv:1508.07774] [INSPIRE].

[35] A. Arbey, F. Mahmoudi, O. Stal and T. Stefaniak, *Status of the Charged Higgs Boson in Two Higgs Doublet Models*, *Eur. Phys. J. C* **78** (2018) 182 [arXiv:1706.07414] [INSPIRE].

[36] D. Chowdhury and O. Eberhardt, *Update of Global Two-Higgs-Doublet Model Fits*, *JHEP* **05** (2018) 161 [arXiv:1711.02095] [INSPIRE].

[37] O. Eberhardt, A.P. Martínez and A. Pich, *Global fits in the Aligned Two-Higgs-Doublet model*, *JHEP* **05** (2021) 005 [arXiv:2012.09200] [INSPIRE].

JHEP07(2021)195